Chapter Fourteen

Laser-Materials Processing for Energy Storage Applications

Heungsoo Kim[1], Peter Smyrek[2,3], Yijing Zheng[2,3], Wilhelm Pfleging[2,3], and Alberto Piqué[1]

[1]Materials Science & Technology Division, Naval Research Laboratory, Washington, DC 20375, USA

[2]Karlsruhe Institute of Technology, IAM-AWP, P.O. Box 3640, 76021 Karlsruhe, Germany

[3]Karlsruhe Nano Micro Facility, Hermann-von-Helmholtz-Platz 1, 76344 Egg.-Leopoldshafen, Germany

This chapter will review the use of laser-based material processing techniques, such as pulsed laser deposition (PLD), laser-induced-forward transfer (LIFT), and materials processing via 3D laser structuring (LS) and laser annealing (LA) techniques for energy storage applications. PLD is a powerful tool for fabricating high-quality layers of materials for cathodes, anodes and solid electrolytes for thin-film microbatteries. LIFT is a versatile technique for printing complex materials with highly porous structures for the fabrication of micropower sources, such as ultracapacitors and thick-film batteries. LS is a recently developed technique for modifying the active material by forming advanced 3D electrode architectures and increasing the overall active surface area. LA is a rapid technology for adjusting the crystalline battery phase and for controlling the grain size on micro and nano scale. This chapter will review recent work using these laser-processing techniques for the fabrication of micropower sources and lessons learned from the characterization of their electrochemical properties.

Book Title
First Author & Second Author

www.panstanford.com

14.1 INTRODUCTION

In the past two decades, there has been significant progress towards developing smaller scale and portable electronic devices, such as autonomous microelectronic sensors, micro-electromechanical systems (MEMS) and portable personal electronics. However, the miniaturization of the power sources required to operate these microscale devices has shown a little progress due to their volumetric 3D characteristics, limiting the ability of these devices to function autonomously. Therefore, the development of micropower systems and small-scale energy storage systems is essential to capitalize on the advantages of miniaturized devices. A lot of techniques have been applied to fabricate microbatteries, such as thin-film, stretchable and three-dimensional (3D) batteries [1-4]. Among many techniques investigated to date, laser-based processes, such as pulsed laser deposition (PLD), laser-induced forward transfer (LIFT) and laser structuring (LS), are useful approaches to integrate various types of micropower sources, such as thin-film microbatteries, ultracapacitors, and solar cells for various microdevices. For the purposes of this review, micropower sources are defined as miniaturized electrochemical cells, such as Li-ion batteries or ultracapacitors, where the total footprint area of the devices is in the mm^2 to cm^2 range, the thickness of the active layers is less than 10 μm (for thin-film batteries) to 10-100 μm (for thick-film batteries), and the total mass of active material does not exceed 10 grams.

The power demand for micropower sources is largely dependent on their anticipated applications. For example, a few μW of power is required for applications, such as MEMS, microelectronic sensors and some small personal electronics [5], while 1-100 μW of power is consumed by radio frequency identification (RFID) tags [6]. In order to meet the power demand for certain types of microdevices, a combination of different types of power sources is required [7]. For example, wireless sensors consume very little power (<1 mW) in stand-by mode, while they consume mW of power in data collection mode, and several hundreds of mW is required to transmit the data to a remote system. In this example, a lithium-ion microbattery can deliver the constant low power (few mW), an ultracapacitor can deliver the short burst of high power and the power sources can be recharged by energy harvesting modules during stand-by mode. As this chapter will show, laser processing techniques are ideally suited to prototype and fabricate these types of electrochemical energy storage components for hybrid micropower systems.

Recently, microbatteries with three-dimensional (3D) architectures have been suggested to enhance the power density while maintaining the high energy density of these systems [8-10]. These proposed 3D configurations can now be realized using laser-based processes to modify the active materials found in 3D Li-ion microbatteries. Furthermore, laser processing techniques can also directly embed the electrochemical components into the device package, leading to a reduction in size and weight of the entire system [11]. Thus, laser-based processing techniques are promising approaches for developing micropower sources for microelectronic devices. This chapter will present a brief review of PLD techniques for thin-film microbatteries, LIFT techniques for ultracapacitors and thick-film microbatteries, and laser structuring processes for modifying active electrode materials for Li-ion microbatteries. Finally, we will conclude with a discussion of challenges and future directions offered by the use of lasers to develop the next generation of microbatteries.

14.2 BACKGROUND AND OVERVIEW OF MATERIALS FOR ENERGY STORAGE

The two main electrochemical energy storage systems used in micro-scale devices are ultracapacitors and microbatteries. Ultracapacitors, also known as supercapacitors, are electrochemical energy storage devices with high power density that can be fully charged and discharged in a very short period of time [12]. Although the energy density of ultracapacitors is lower than that of microbatteries, they can deliver the stored energy in a very short time and can be charged/discharged millions of times without losing their energy storage capacity. Ultracapacitors can be classified into two possible classes based on their charge storage mechanisms or the type of their electrode materials. The first category is electrochemical double layer capacitors that can store charge electrostatically on the electrode-electrolyte interface. Carbon materials are commonly used in this type of ultracapacitors because they provide high surface area and accordingly a large amount of charge storage in the system. The second category is pseudo-capacitors or redox capacitors, which store charge through surface redox reactions. Transition metal oxides are typical examples of pseudo-capacitors [12]. Both types of ultracapacitors show typical capacitor behavior: at constant current, the voltage across the device will decrease linearly with time.

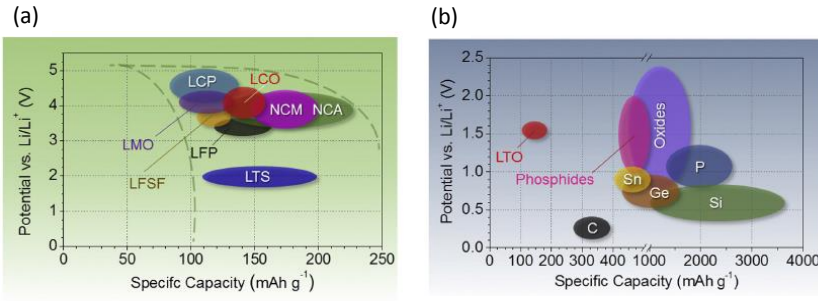

Figure 14.1. Discharge potentials vs. specific capacity of some of the most commonly used (a) cathode and (b) anode active materials. The acronyms represent as follows: LCO for $LiCoO_2$, LMO for $LiMn_2O_4$, NCM for $LiNi_{1/3}Co_{1/3}Mn_{1/3}O_2$, NCA for $LiNi_{1/3}Co_{1/3}Al_{1/3}O_2$, LFP for $LiFePO_4$, and LTS for $Li_4Ti_5S_{12}$. Reprinted from [13], Copyright (2015), with permission from Elsevier.

Rechargeable Li-ion batteries (LIBs) have been considered as the most promising energy storage system due to their highest energy per unit weight within the known energy storage systems. The commonly used cathode materials in LIBs are transition metal oxides or phosphates ($LiCoO_2$, $LiMn_2O_4$, $LiNi_{1/3}Mn_{1/3}Co_{1/3}O_2$, $LiNi_{1/3}Co_{1/3}Al_{1/3}O_2$, and $LiFePO_4$), while graphite is the most commonly used anode material. Both electrodes are separated by a polypropylene membrane filled with electrolyte that contains lithium salts such as $LiPF_6$. The separator blocks the electrical contact between the electrodes while it allows the diffusion of Li-ions during the charging/discharging processes. Figure 14.1 provides a graphical comparison of the performance of various active electrode materials used in LIBs [13] In general, the higher the specific capacity the better while higher potentials allow for higher power operation.

Although graphite is the most commonly used anode material in LIBs due to its low working potential, good cycle life and low cost, it allows only one Li ion with six carbon atoms for intercalation. Thus, its low reversible capacity (372 mAh g^{-1}) cannot meet high capacity demand of many electronic devices. There have been many efforts searching for new anode materials for Li-ion batteries. Among them, silicon has been considered as the most attractive anode material due to its high theoretical capacity ($Li_{22}Si_5$, 4000 mAh/g) and its abundance [14]. However, its application suffers from the significant inhomogeneous volume expansion in silicon during insertion and extraction of Li-ions. This volume expansion quickly destroys the electrical contacts in the Si anode after a few initial

cycles. Therefore, it is necessary to develop ways to use Si while maintaining its conductivity. Some efforts to overcome these limitations using laser-based processes will be discussed in this chapter.

14.3 GROWTH OF ENERGY STORAGE MATERIALS BY PULSED LASER DEPOSITION (PLD)

Figure 14.2 shows a schematic illustration of the basic components for a PLD setup. A UV excimer laser, such as ArF (193 nm), KrF (248 nm) and XeCl (308 nm) is utilized with a pulse width of tens of nanoseconds or shorter. Other types of lasers, such as the various harmonics of a Nd:YAG laser, have also been employed for PLD. The PLD process is very simple. A pulsed laser beam is used to evaporate material from a target forming a thin film on a substrate retaining the target composition. The high-power laser beam is focused inside a vacuum chamber onto the target typically at an incident angle of 45°. The target is typically rotated in order to avoid its fast deterioration and keep its surface under approximately constant conditions. The ablation of the target produces a visible plasma plume that expands from the target to the substrate. The target-to-substrate distance is in the range of 4 - 10 cm. This process can be performed in any kind of inert or reactive atmosphere and also performed at a dynamic range of pressures from ultra-high vacuum (UHV) to high pressures (typically up to 1 Torr). An

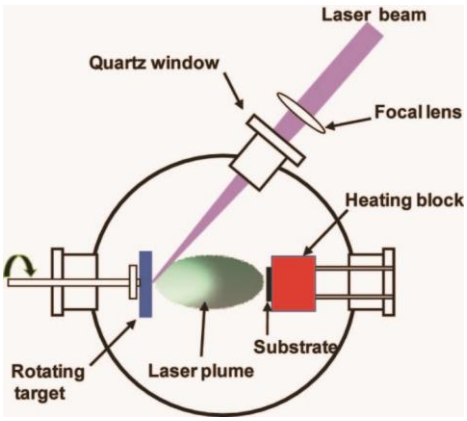

Figure 14.2. A schematic illustration of the pulsed laser deposition setup.

important feature of the PLD technique is its capability to deposit multilayer thin films using a multi-target carousel system. The laser beam can be alternatively focused over two or more targets, inducing a sequential ablation process. This configuration is well suited for manufacturing complex stacks such as typical layered battery structures.

Another advantage of PLD is that the deposited films have compositions close to the targets. This is a result of the extremely high heating rates absorbed by the target surface due to its strong interaction with the laser irradiation. At low laser fluences, the laser pulse simply heats the target and evaporates the target species. In this case, the evaporative flux from a multicomponent target can be determined by the vapor pressures of its constituents. As the laser fluence is raised above the ablation threshold where the absorbed laser energy becomes higher than that needed for evaporation, the flux of vaporized species is independent of the vapor pressures of its constituents. This non-equilibrium process induces the congruent evaporation of the target. This stoichiometry transfer between target and substrate is difficult to achieve with other physical vapor deposition techniques such as sputtering.

14.3.1 *PLD of Cathodes*

The PLD technique has been used to grow various cathode materials, such as $LiCoO_2$ and $LiMn_2O_4$ for Li-ion microbatteries. An ideal thin-film cathode in a Li-ion microbattery is a layered structure of lithiated oxides with a well crystallized structure. The film crystallinity can be improved by a post-deposition annealing, which is often required at relatively high temperature. However, this high temperature annealing process may produce microcracks in the cathode films, resulting in non-uniform surface morphology of the solid electrolyte in the sequential deposition step and consequently shorting problem in the thin-film microbatteries. Therefore, it would be great if a crystallized $LiCoO_2$ thin-film cathode could be deposited without a high temperature annealing step. One of the important features in PLD is that the kinetic energy (10 to 100 eV) of the ejected species in the laser-induced plasma plume is much higher than those from other physical vapor deposition techniques such as sputtering (5 to10 eV) or evaporation (< 1 eV) [15-17]. Thus, $LiCoO_2$ cathode films grown by PLD technique can be crystallized at relatively low temperatures (300 – 600 °C) without any post deposition annealing, compared to other physical vapor deposition techniques (600 – 800 °C) [18-21]. It was reported that PLD grown $LiCoO_2$ thin films are single phase and well-crystallized structures with high

density and smooth surfaces without cracks, which are essential for high performance in thin-film batteries [22].

The crystallographic orientations of the cathode thin-films is another key parameter that affects the electrochemical activity. In PLD, the high supersaturation of the ablated flux creates 2D island nucleation on the film surface, which is suitable for layer-by-layer growth mode to form highly oriented thin-films [16]. In PLD of the $LiCoO_2$ cathode thin films, the grains with (003) preferred orientation tend to reduce the Li-ion diffusivity while the grains with (101) and (104) orientations increase the Li-ion diffusion [23]. The substrate is also an important parameter to determine the microstructure of the cathode films. $LiNi_{0.5}Mn_{0.5}O_2$ cathode thin films were grown by PLD on two different substrates (stainless steel and Au) [24]. The films grown on stainless steel substrate formed a spinel structure, whereas the films grown on Au substrate showed a layered structure. The reversible capacity of the $Li/LiNi_{0.5}Mn_{0.5}O_2$ battery on the Au substrate showed ~150 mAh/g (between 2.5 and 4.3 V), which is close to the theoretical capacity (~160 mAh/g) and is much higher than that of the stainless steel substrate (~40 mAh/g between 2.5 and 4.5 V).

Although one of advantages of PLD is that the stoichiometry of the films is normally close to that of the targets, it is not the case when the targets contain volatile light elements such as lithium [25]. In the case of lithium containing targets, the lithium content in the deposited films tends to be lower than that in the targets because these light elements are easily scattered by background gas molecules or other species in the plasma. This Li-content deficiency in the deposited film leads to structural changes and impurity formation, which will eventually degrade the battery performance. This problem can be resolved by using targets containing excess Li_2O [18,23,25]. Simmen *et al*. reported that $LiMn_2O_4$ cathode thin-films with a desired lithium content can be achieved using a composite target of $Li_{1.03}Mn_2O_4$ and 7.5 mol% Li_2O [25] with a discharge capacity of ~42 $\mu Ah/cm^2$-µm. It was also reported that textured $LiCoO_2$ cathode thin films were also successfully prepared by a $LiCoO_2$ target containing 15% excess Li_2O and their batteries showed reasonably good electrochemical performance (~50-60 $\mu Ah/cm^2$-µm) [23].

As discussed before, crystallinity, smooth surface morphology, composition and preferred orientation of the cathode films are very important conditions to produce high quality cathode thin films. **Table 1** shows electrochemical properties of thin-film cathodes prepared by PLD reported in the literature.

Table 1. Electrochemical properties of thin-film cathodes and anodes prepared by PLD. SS represents the stainless steel.

Material	Substrate	Voltage/Current	Capacity	Ref.
Cathode				
$LiCoO_2$	SiO_2/Si	3.0-4.2V/ 15 μA/cm^2	64 μAh/cm^2-μm	[20]
$LiCoO_2$	SnO_2/glass	3.8-4.2V/ 5μA	89 mAh/g	[26]
$LiCo_{0.5}Al_{0.5}O_2$	SnO_2-glass	3.8-4.2V/ 5μA	30 mAh/g	[26]
$LiNi_{0.8}Co_{0.2}O_2$	-	3.0-4.3V/ 10 μA/cm^2	125 mAh/g	[27]
$LiNi_{0.8}Co_{0.15}Al_{0.05}O_2$	Si, Ni	2.5-4.2V/ ~5 μA/cm^2	98 μAh/cm^2-μm	[28]
$LiFePO_4$-C	Pt/Si	2.0-4.0V/ ~8 μA/cm^2	20 μAh/cm^2-μm	[29]
$Li_{1.13}Mn_2O_{3.73}$	SS	3.5-4.4V/ 2C rate	30 μAh/cm^2-μm	[25]
$LiNi_{0.5}Mn_{0.5}O_2$	Au	2.5-4.3V/ 2 μA/cm^2	150 mAh/g	[24]
$LiNi_{0.5}Mn_{0.5}O_2$	SS	2.5-4.5V/ 2 μA/cm^2	40 mAh/g	[24]
$Li_{1.2}Mn_{0.54}Ni_{0.13}Co_{0.13}O_2$	Au	2-4.8V/ 2 μA/cm^2	70 μAh/cm^2-μm	[30]
Anode				
Si-C	Cu	0.05-1.5V/ 54 μA/cm^2	70 μAh/cm^2	[31]
Si-graphene	Ni	0.05-1V/ C/5 rate	2400 mAh/g	[32]
a-Si	Si,SS	0.01-1.5V/ 100 μA/cm^2	64 μAh/cm^2	[23]
a-SnO	-	1.5-2.7V/ 100 μA/cm^2	4-10 μAh/cm^2	[33]

14.3.2 *PLD of Anodes*

Although graphitized carbon is the most commonly used anode material in lithium-ion batteries, its low theoretical capacity (i.e. LiC_6, 372 mAh/g) cannot meet the capacity demand of batteries in many electronic devices. There have been many research efforts on searching for new anode materials for Li-ion batteries. Among them, silicon has been considered as the most attractive anode material due to its high theoretical capacity ($Li_{22}Si_5$, 4000 mAh/g) and its abundance [34]. However, its application suffers from the significant

inhomogeneous volume expansion in silicon during insertion and extraction of Li-ions, leading to fast capacity fading. Amorphous silicon (a-Si) material has been studied as a promising anode for Li-ion batteries due to its homogeneous volume expansion during lithium insertion and accordingly improved cycling performance [35]. The a-Si anode thin films were successfully grown on stainless steel substrates at room temperature by PLD (KrF excimer laser, 248nm) [23]. The 120 nm thick a-Si anode thin-films showed a reversible capacity of 64 μAh/cm^2 between 0.01 and 1.5 V with a stable cycling behavior for 50 cycles with a small fade rate in capacity of 0.2% per cycle. The a-Si/$LiCoO_2$ cell exhibited a stable discharge capacity of ~20 μAh/cm^2 between 1 and 4 V for 20 cycles [23]. Table 1 shows some of the electrochemical properties of the a-Si anode thin-films. The film thickness also affects the cycle life of the a-Si anode thin-film. As the film thickness increases, capacity fading occurs faster due to increased Li-ion diffusion length.

PLD was also utilized to deposit thin Si layers on a multilayer graphene (MLG) coated Ni foam substrate to build a Si-MLG composite anode for Li-ion batteries [32]. The MLG layer, first grown by chemical vapor deposition, serves as a conducting platform, thereby preventing contact loss from volume expansion during charging/discharging processes for the Si anode. The Ni foam substrate serves as a current collector and provides large surface area compared to thin metal foils. The cells based on the Si-MLG anodes displayed a stable capacity of ~2400 mAh/g during cycling test, whereas the cells on the pure Si anodes showed higher capacity during the first cycle (~2800 mAh/g) but their capacity faded rapidly during subsequent cycles. Thus, this combination of silicon and graphene offers an alternative route for reducing volume expansion issues on Si anodes. Recently, Biserni et al fabricated composite Si-C anodes by depositing nanostructured porous a-Si films by PLD at room temperature, followed by CVD of a thin carbon coating. [31]. The mesoporosity of nanostructured Si film helps to reduce the volume expansion issues, while the thin CVD grown carbon layer helps to promote the formation of a stable solid electrolyte interface (SEI) layer and protect the Si from direct contact with the electrolyte. The cell based on these composite Si-C anodes exhibited a capacity of ~75 μAh/cm^2 after 1000 cycles at a current rate of 540 μA/cm^2, indicating their excellent capacity retention and cycle performances (see Fig. 14.3).

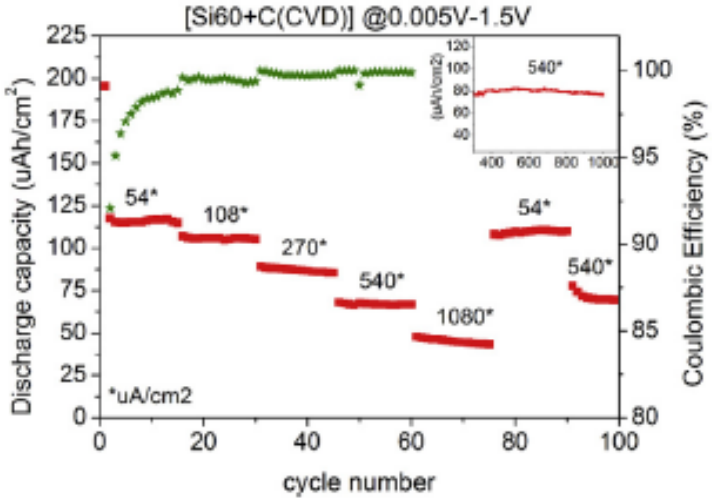

Figure 14.3. Curves of discharge capacity (square, red) and coulombic efficiency (star, green) of Si-C anodes. Integer numbers within the graphs represent the constant current rates (μAcm^{-2}) applied during test. The inset shows cycle performance of the Si-C anode at a constant current rate of 540 $\mu A\ cm^{-2}$ for 1000 cycles. Reprinted from [31], Copyright (2015), with permission from Elsevier.

In addition, PLD can also be used to generate more complex Si anodes comprising multilayer stacks, sandwiched structures or layers with a controlled gradient in composition. Such non-uniform geometries might help minimize cracking and delamination through improved handling of the large volume expansion of the silicon, thus resulting in improved cycling performance of the silicon anodes. **Table 1** lists the electrochemical properties of thin-film anodes prepared by PLD. Although significant improvement has been reported on the Si-based anode thin-films, their properties, such as cycle life, high rate, capacity retention, and film thickness, must be improved before it is used as a reliable anode material.

14.3.3 *PLD of Solid-State Electrolytes*

A solid-state electrolyte is one of the key materials for fabricating thin-film Li-ion batteries since there is a safety issue on traditional Li-ion batteries that use

highly flammable organic liquid electrolytes. There have been considerable studies on all solid-state thin-film type Li-ion batteries using nonflammable solid electrolytes due to their excellent potential for improving their safety and reliability. The PLD technique has been utilized in growing various inorganic solid-state electrolytes, such as lithium phosphorous oxynitride (LIPON), $Li_{2.2}V_{0.54}Si_{0.46}O_{3.4}$ (LVSO), Li_4SiO_4-Li_3PO_4, $Li_{3.25}Ge_{0.25}P_{0.75}S_4$ (*thio*-LISICON) and Li_2S-P_2O_5 films [33, 36-41]. Ideally, the solid-state electrolyte should have high ionic conductivity and low electronic conductivity for thin-film batteries. **Table 2** shows data from various solid-state electrolyte thin-films prepared by PLD. LIPON was successfully deposited by PLD and showed that the ionic conductivity can be adjusted with the concentration of nitrogen in the films by changing the N_2 background gas pressure during deposition [36]. The Li-ion conductivity of the PLD grown electrolyte films ranges from 10^{-4} to 10^{-7} S/cm while the electric conductivity ranges from 10^{-7} to 10^{-13} S/cm. Due to their high Li-ion conductivity and low electron conductivity, these PLD grown solid-state thin-film electrolytes are promising for developing all solid-state Li-ion microbatteries.

Table 2. Electrochemical properties of electrolyte thin-films prepared by PLD.

Material	Substrate	Li-ion conductivity (S/cm)	Reference
LiPON	Si, Au/Si,	$1.6x10^{-6}$	[36]
$Li_{2.2}V_{0.54}Si_{0.46}O_{3.4}$ (LVSO)	quartz	$2.5x10^{-7}$	[33]
$Li_{6.16}V_{0.61}Si_{0.39}O_{5.36}$ (LVSO) [a)]	Si, Al/glass	$3.98x10^{-7}$	[37]
$Li_{3.4}V_{0.6}Si_{0.4}O_4$ (LVSO)	Si, fused silica	10^{-7}	[38]
$Li_{3.25}Ge_{0.25}P_{0.75}S_4$ (thio-LISCON)	quartz	$1.7x10^{-4}$	[39]
$80Li_2S$-$20P_2S_5$	Si	2.8×10^{-4} [b)]	[40]
Li_4SiO_4-Li_3PO_4	quartz	$1.6x10^{-6}$	[41]

a) The target composition.

b) Heat treated at 200 ºC for 1hr.

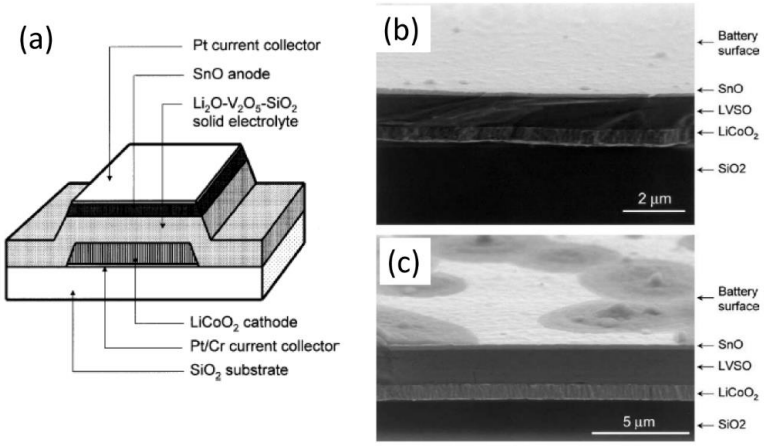

Figure 14.4. (a) Schematic illustration of a thin film Li-on battery. SEM micrographs showing cross-sectional vies of thin flm LI-ion batteries: (b) before and (c) after 100 cycles at a current density of 44 μAh cm^2. Reprinted from [33], Copyright (2004), with permission from Elsevier.

Another advantage of PLD in fabricating thin-film batteries is that all solid-state thin-film layers can be fabricated by sequential PLD process. For example, all solid-state thin film microbatteries, consisting of $LiCoO_2$ cathode, LVSO solid electrolyte and amorphous SnO anode, were fabricated by sequential PLD process [33]. A schematic cross-sectional view of this thin-film Li-ion battery is shown in Fig. 14.4(a). Figs. 14.4(b) and 14.4(c) show SEM micrographs of cross-sectional views of the batteries before and after testing for 100 cycles. The interface between the $LiCoO_2$ cathode, LVSO electrolyte and the SnO anode remained smooth before and after cycling test. This thin-film microbattery showed an initial discharge capacity of 9.5 μAh/cm^2 and 45 % of initial discharge capacity was retained after 100 cycles at a constant current rate of 44 μA/cm^2 between 0.01 and 3 V [Fig. 14.4].

In summary, PLD is a powerful technique for fabricating high-quality layers of materials for cathodes, anodes and solid electrolytes for thin-film microbatteries. Due to the relatively low crystallization temperature, highly textured cathode films can be prepared by PLD. PLD has been successfully employed to deposit amorphous silicon, silicon-graphene and Si-C composite anodes, while various solid-state thin-film electrolytes have been fabricated by PLD with high Li-ion conductivity and low electronic conductivity. Finally, all

solid-state thin-film microbatteries have been demonstrated by applying sequential PLD growth. In addition, from an applications point of view, fabricating thin film microbatteries on flexible plastic substrates is highly desirable. However, most of the cathode and anode thin films are required to be grown at elevated temperatures (500 – 600 °C). This is one of the limitations of thin-film batteries grown by physical vapor deposition techniques such as e-beam and sputtering. However, since films grown by PLD can be crystallized at relatively low temperatures, it might be possible to grow active materials by PLD at relatively low temperatures (<300 °C) on flexible substrates such as polyimide (Kapton).

14.4 PRINTING OF ENERGY STORAGE MATERIALS BY LASER-INDUCED FORWARD TRANSFER (LIFT)

LIFT is a direct write technique that allows high resolution printing from a variety of functional materials. Figure 14.5 shows a schematic illustration of the basic elements for the LIFT process. The concept of the LIFT process is simple. It uses a pulsed laser beam to induce the transfer of material from a donor substrate onto a receiver substrate. The donor substrate is prepared by coating the material of

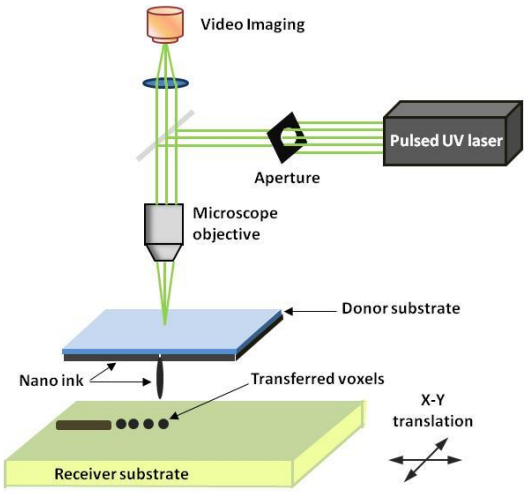

Figure 14.5. A schematic illustration (not to scale) of the laser-induced forward transfer (LIFT) setup.

interest onto a laser-transparent quartz wafer and is also referred to as the ribbon. The receiver substrate is placed on the x-y stage facing the donor substrate at a distance of tens of microns. Laser pulses are focused onto the donor film by a microscope objective. When the incident laser pulse is higher than the threshold energy, material is ejected from the ribbon and transferred to the receiver substrate. Typical laser fluences for LIFT of battery materials, depending on the donor film thickness, range from 10 to 100 mJ/cm^2. In general, the laser beam is traveled by galvanometric scanning mirrors for the fast pattern generation during the LIFT process and a computer-controlled X-Y motion control system translates the ribbon and receiving substrates. A CCD camera can provides a real-time plan view of the transfer process. Unlike other film deposition and patterning processes, LIFT processes can be performed at ambient conditions without using vacuum or clean-room environments.

One of the advantages of LIFT is that the deposited materials typically show porous structures with high surface areas. These porous structures are very important features for electrochemical devices due to an increased contact area between the electrodes and the electrolyte, leading to improved charge transfer and accordingly a more complete utilization of the electrode materials. Thus, the LIFT technique is ideally suited for printing the active electrodes in most energy storage systems, such as batteries, capacitors and solar cells [42-49]. Another important feature of the LIFT process is that unlike inkjet printing, the LIFT technique is suitable to print high viscosity nanoinks due to its nozzle-free nature [50,51]. Although the inkjet printing is a simple technique, inkjet printing is limited by the transfer of only low viscous nanoparticle suspensions in order to avoid clogging of the dispensing nozzles [53]. Thus, printing of precise patterns by inkjet is very difficult due to the variable behavior of fluids on different types of surfaces and their unstable wetting effects [54, 55]. Recently, LIFT has been applied to print high viscosity pastes by laser-decal transfer (LDT) [56-63]. The LDT process is a new type of direct-writing techniques in which voxel shape and size become controllable parameters, allowing the creation of thin-film like structures for a wide range of applications, such as 3D interconnects, free-standing structures, metamaterials, membranes and circuit repair. Furthermore, the complex shapes can be printed by a single laser pulse in one step, reducing the processing time and avoiding problems related to the merging of multiple voxels. Thus, in the case of small scale energy storage, LIFT is beneficial as it can directly print the active materials into the substrate housing the circuit, i.e., embedding the entire micropower source, eliminating excess weight due to packing.

In addition, by combining LIFT with a digital micro-mirror device, the size and shape of an incident laser beam can be dynamically controlled in real time, resulting in laser-printed functional materials with geometries identical to those of the projected beam [57, 62]. In this section, the use of LIFT techniques will be demonstrated to process active electrochemical materials for the fabrication of various micropower systems, including ruthenia-based planar ultracapacitors, rechargeable thick-film Li-ion microbatteries and solid-state electrolyte membranes.

14.4.1 *LIFT of Ultracapacitors*

The LIFT technique has been successfully employed to fabricate ultracapacitors [46,64]. An ultracapacitor is another type of electrochemical energy storage and power generation system that displays electronic properties similar to both battery and capacitors. Like a battery, it has the ability to store a large amount of energy during charging state and like a capacitor, an ultracapacitor has the ability to discharge its energy very rapidly with high power density. Thus, the ultracapacitor, like a battery capable of high discharge rates, is typically used for load leveling and applications where a short burst of power is needed. Hydrous ruthenium oxide is an excellent electrode material for micro-ultracapacitor due to its high specific capacitance. A large pseudocapacitance effect can be achieved by rapid insertion and release of electrons and protons through this material due to its high specific surface area [65]. This effect can be enhanced by the creation of structural water in the lattice, providing more percolation pathways for proton conduction into the material [66]. The chemistry of this system involves two identical electrodes composed of a hydrous metal oxide whose electrochemical performance is sensitive to the processing temperature [67]. One of the important features of LIFT is that it can print ink composed of the electrode material and relevant electrolyte. Arnold *et al* [46] demonstrated a planar type of hydrous ruthenium oxide ultracapacitors using the LIFT process with significantly improved discharge behavior. The active ink was composed of hydrous ruthenium oxide powder and sulfuric acid electrolyte. As shown in Figs. 14.6(a,b), a 1 cm^2 gold-coated glass substrate laser micromachined into four electrically isolated region serves as the electrodes for the cells. Fig. 14.6(c) shows a typical charge/discharge plots for these ultracapacitor cells. The cell is charged at 50 μA until the voltage across the cell reaches 1V. A constant current was applied during discharging until the voltage returns to zero. The cells exhibited the linear charge/discharge behavior at constant current, indicating ideal capacitor behavior.

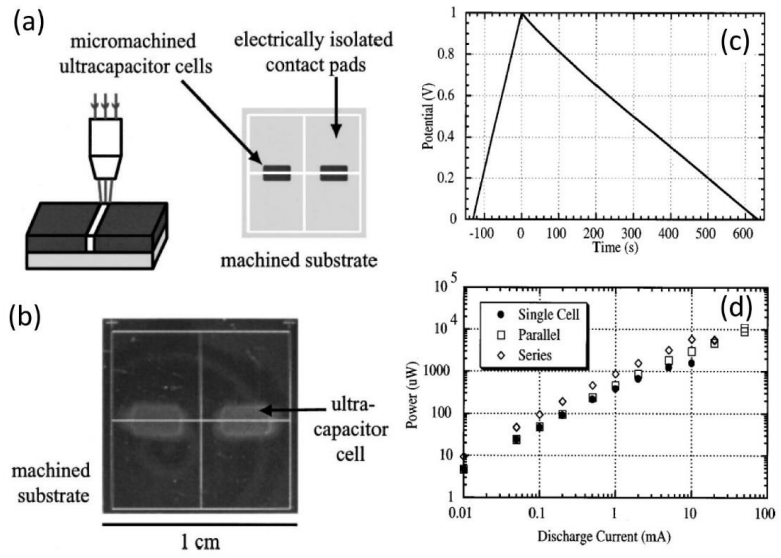

Figure 14.6. (a) Micromachining to produce a planar RuO_2-$0.5H_2O$ micro-ultracapacitor. (b) Picture laser machined planar microultracapacitors on gold-coated quartz substrate. (c) Plot showing the charging/discharging behavior of hydrous ruthenium oxide ultracapacitor printed by LIFT. Cell is charged at 50 µA and discharged at 10 µA. Starting lines are indicative of ideal capacitor behavior. Total electrode mass is 100 µg with a footprint of $2mm^2$. (d) Power as a function of discharge current for a single ultracapacitor cell as well as parallel and series combinations. The power is calculated over 0-1V for the single cell and parallel combination, and 0-2V for the series combination. [64] (Reproduced by permission of The Electrochemical Society).

Fig. 14.6(d) shows that the ultracapacitors added in series and parallel can be discharged at currents above 50 mA without damaging the cells [64].

14.4.2 *LIFT of Li-ion Microbatteries*

LIFT technique has been successfully employed to print thick-film electrodes for microbatteries with much higher capacities per electrode area than those made by sputter-deposited thin-film electrodes [42-47]. This enhanced performance is related to the previously mentioned porous structure of the layers typically printed by LIFT. This porosity is what allows improved diffusion of the Li-ions across the electrodes without a significant internal resistance loss. Kim *et al* fabricated thick-film electrodes ($LiCoO_2$ cathode and carbon anode) by LIFT for Li-ion

microbatteries to study their electrochemical properties [42]. The laser-printed electrodes were separated by a laser-cut porous membrane that is soaked with gel polymer electrolyte to build mm-size solid-state packaged Li-ion microbatteries. Figs. 14.7(a) and 14.7(b) show a cross sectional schematic diagram and SEM micrograph of a typical Li-ion microbattery fabricated by LIFT.

One of the advantages of LIFT is that the thickness of the printed films can be easily adjusted by the number of LIFT printing passes. For example, the thickness and mass of the $LiCoO_2$ cathode thick-films increase linearly with the number of LIFT passes (see Fig. 14.7(c)). Accordingly, the discharge capacities can also be easily controlled by the number of LIFT passes (see Fig. 14.7(d)). The viscosity of the ink also influences the film thickness, i.e., for high viscosity inks, thicker films are deposited than with lower viscosity inks. With increasing ink viscosity, the laser power required for their printing increases as well, which can

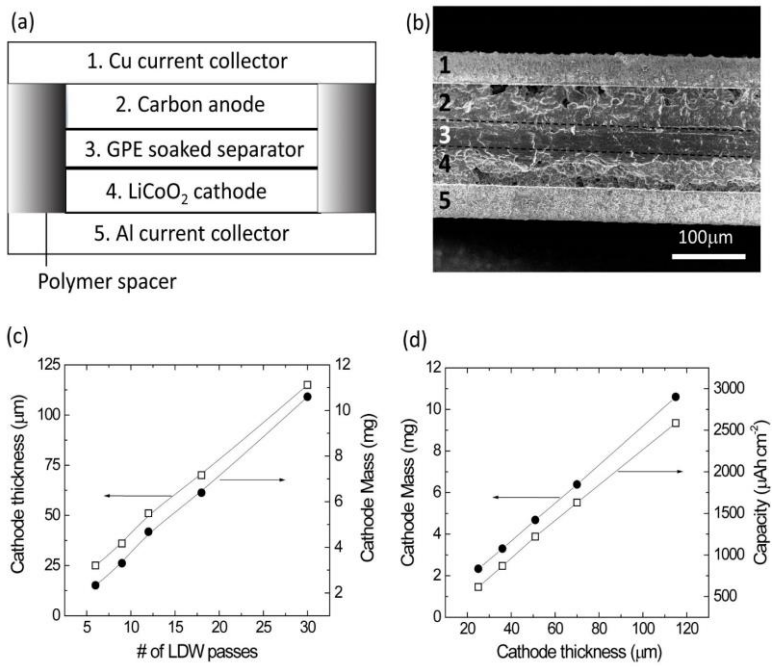

Figure 14.7. (a) Cross sectional schematic diagram of a typical Li-ion microbattery. (b) Cross sectional SEM micrograph of a packaged thick-film Li-ion microbattery. (c) $LiCoO_2$ cathode thickness vs. cathode mass as a function of the number of LIFT passes. (d) $LiCoO_2$ Cathode mass vs. discharge capacity as a function of the cathode thickness. Reprinted from [42], Copyright (2007), with permission from Elsevier.

affect the printing resolution, as well as alter the film components, thus requiring optimization of the transfer conditions for each material.

The electrochemical properties of Li-ion microbatteries based on the laser-printed $LiCoO_2$ cathode thick-films are highly dependent on the cathode thicknesses. Fig. 14.8(a) shows charge/discharge curves at the 5^{th} cycle for Li-ion microbatteries with laser-printed $LiCoO_2$ cathodes of different thicknesses (35 – 115 μm). Microcarbon microbeab (MCMB) graphite is used as an anode layer and a polyolefin-based microporous membrane soaked with a gel polymer electrolyte is used as a separator for these microbatteries. The microbatteries are charged and discharged at a constant current of 100 $\mu A/cm^2$. As shown in Fig. 14.8(a), the discharge capacity per active electrode area is proportional to the cathode film thickness, suggesting that the discharge capacity increases with the cathode thickness (up to 115 μm thick). This increased capacity is related to their high-surface-area porous structure, allowing better ionic and electronic transport through the thick electrodes (~ 115 μm) without any significant internal cell resistance. Fig. 14.8(b) shows the cycle performance of the Li-ion microbattery with 35 μm thick $LiCoO_2$ cathode. The microbattery shows excellent cycling performance over 200 cycles with a slow fade rate. The battery retains about 80% of their initial capacity after 200 cycles. The specific capacity based on the cathode mass shows ~100 mAh/g after 200 cycles (see Fig. 14.8(b)).

The discharge rate is also one of the important properties of the electrodes, especially for high power density applications. Fig. 14.8(c) shows the discharge capacity per active area for $LiCoO_2$ thick-film microbatteries with three different thicknesses (21, 45 and 68 μm) as a function of discharge current rate. The slopes of the curves for all the cells are approximately parallel for current densities between 100 and 2000 $\mu Ah/cm^2$, indicating that the discharge rate is not limited by the cathode thickness for Li-ion transport during discharging. This suggests that the energy per unit area can be increased simply by increasing the thickness of the electrodes without any significant internal resistance loss. The cell with the 68 μm thick cathode produces a maximum power density of ~ 38 mW/cm^2 (~102 $\mu Ah/cm^2$) at a discharge current of 10 mA/cm^2. For the entire current density ranges, almost the same fraction of active material in all the cells is accessed for charge/discharge activities (see Fig. 14.8(d)). These results confirm that the cathode thickness is not a rate limiting factor for the thick-film microbatteries prepared by LIFT due to the porous structure of the laser-printed electrodes.

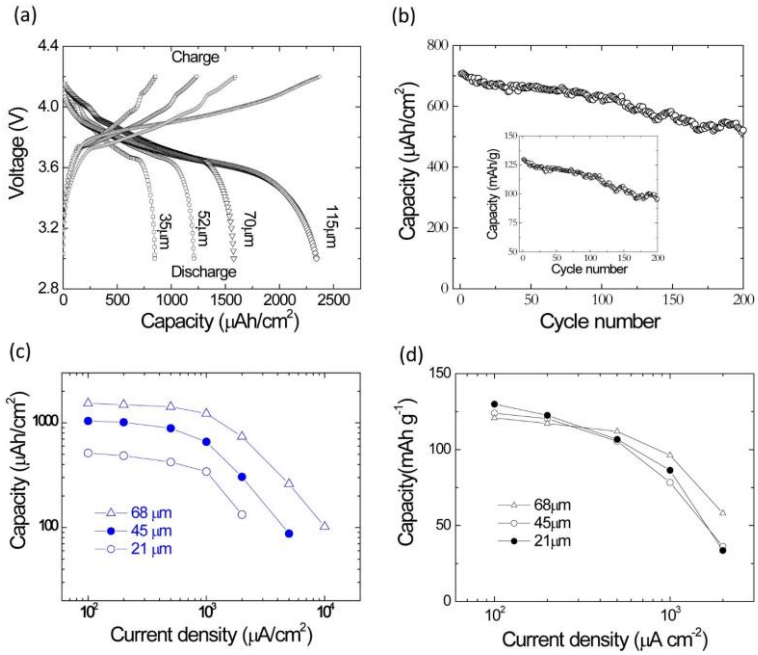

Figure 14.8. (a) Voltage versus capacity per unit area for Li-ion microbattery with different thickness of $LiCoO_2$ cathodes. (b) Cycle performance of the Li-ion microbattery with 35 μm thick $LiCoO_2$ cathode. Discharge capacity per (c) active electrode area and (d) cathode mass for the packaged thick-film microbatteries with three cathode thicknesses (21, 45, and 68 μm).The active electrode area was 0.49 cm^2. Microbatteries were charged at 0.1 mA/cm^2 between 4.2 and 3 V. Reprinted from [42], Copyright (2007), with permission from Elsevier.

It is worth to compare the properties of the laser-printed thick-film electrodes with those of sputter-deposited thin-film electrodes. For example, when we consider the discharge capacity per active electrode area, sputter-deposited 2.5 μm thick $LiCoO_2$ cathodes (active area = 1 cm^2) exhibited a capacity of 160 $\mu Ah/cm^2$ (or ~64 $\mu Ah/cm^2$-μm) at a current density of 100 $\mu A/cm^2$ [4], while the laser-printed 115 μm thick $LiCoO_2$ cathodes (active area = 0.49 cm^2) demonstrated a capacity of 2586 $\mu Ah/cm^2$ (or ~22.5 $\mu Ah/cm^2$-μm) at the same current rate. Despite three times smaller volumetric capacity than that of the sputter-deposited thin-film cells, the laser-printed thick-film microbatteries can produce order of magnitude higher capacities per unit area. Specifically, in order to achieve the same discharge capacity (2586 $\mu Ah/cm^2$) of the 115 μm thick laser-

printed $LiCoO_2$ cathodes employing 0.5 cm^2, the sputter-deposited 2.5 μm thick $LiCoO_2$ cathodes would have to occupy an area of ~8 cm^2. Based on this comparison, it is clear that the laser-printed thick-film microbatteries are well suited for applications where limited space is available for the power source such as wireless network sensors or autonomous microelectronic devices.

14.4.3 *LIFT of Solid-State Electrolytes*

A liquid electrolyte is mostly used in commercial Li-ion battery systems due to its high ionic conductivity. However, the use of the liquid electrolyte is limited by leakage and safety issues. In order to resolve these limitations it is important to replace the liquid electrolyte with a solid-state polymer electrolyte since the volatility of the liquid electrolyte is no longer a concern. This solid-state polymer electrolyte would allow for easier packaging with less material. Ollinger *et al* reported on the printing by LIFT of an ionic liquid based nanocomposite solid-state electrolyte for the fabrication of Li and Li-ion microbatteries [43,44]. The key feature of this solid-state electrolyte is that the laser-printed solid-state membranes exhibited the proper electrochemical behavior for ionic liquids with a high ionic conductivity of 1- 3 mS cm^{-1}, while maintaining the strength and flexibility of the PVD-HFP co-polymer matrix. Accordingly, they can serve as both the electrolyte and separator [43]. Fig. 14.9(a) shows the optical micrographs of laser-printed solid-state polymer membranes on a glass substrate. These laser-printed membranes were dried at 75 ºC for 1 hour forming a continuous flexible pinhole free membrane. It is clear from these micrographs that even 5 μm thick membranes were strong enough and flexible enough to be lifted off using tweezers without damaging the membranes (see Fig. 14.9b). Fig. 14.9(c) shows the first 4 cycles for a Li-ion microbattery fabricated with the laser-printed solid-state membrane (~20 μm thick), the 30 μm-thick $LiCoO_2$ cathode and the Li-metal anode. The LIFT process was also employed to print sequential layers of cathode ($LiCoO_2$), solid-state electrolyte, and anode (MCMB graphite) into a laser-micromachined pocket on a thin polyimide substrate (Kapton) to build an embedded all solid-state Li-ion microbattery [11]. This microbattery was charged and discharged at C/3 rate (~110 μA/cm^2) and exhibited an energy density of 1.32 mWh/cm^2 (or 0.41 mWh/cm^3) corresponding to a specific energy of 330 mWh/g (~ 100 mAh/g).

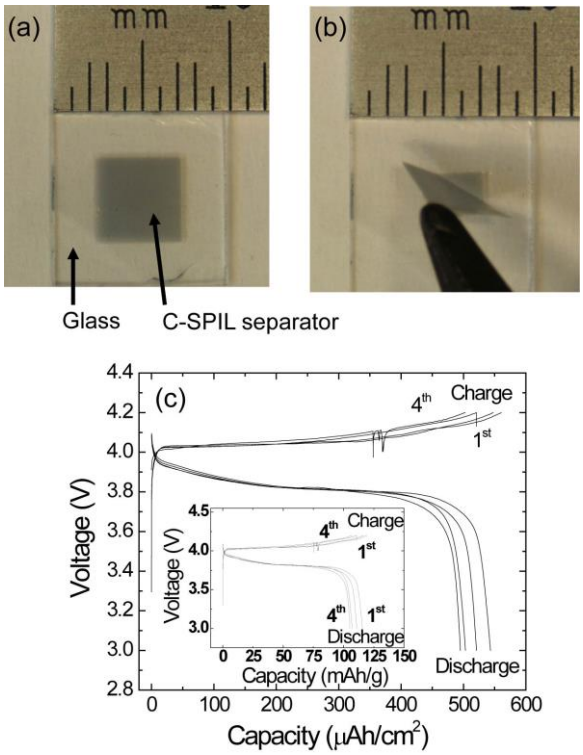

Figure 14.9. Optical micrographs of (a) the laser-printed c-SPIL membranes on a glass substrate and (b) membrane partially lifted off of glass slide by tweezers. (c) Charge-discharge performance of a packaged Li microbattery ($LiCoO_2$/c-SPIL separator/Li) cycled between 4.2V and 3V at current density of 40 μA/cm^2. The battery was tested in air at 25°C. The active electrode area is 1cm^2. Reprinted from [43], Copyright (2006), with permission from Elsevier.

14.5 3D PROCESSING OF ENERGY STORAGE MATERIALS BY LASER STRUCTURING (LS) AND LASER ANNEALING (LA)

The development of three-dimensional (3D) architectures for electrodes in lithium-ion batteries is a promising approach to overcome problems such as 1-dimensional lithium-ion diffusion, inhomogeneous current densities, power losses, high inter-electrode ohmic resistances as well as mechanical stresses due

to high volume changes resulting from de/lithiation during charging and discharging processes. By applying 3D battery architectures, one can achieve large areal energy capacities while maintaining high power densities at the same time. This feature is important, e.g. for thin film batteries where the lithium-ion diffusion is limited by the thickness of the compact film. A common approach for realization of 3D architectures in electrodes is the structuring of the current collector. An increased active surface achieved by 3D electrode architectures can induce large areal energy densities. Unfortunately, this approach is in a very early stage of development and in general it is not feasible for state-of-the-art electrodes.

With the direct structuring of thick and thin film electrodes, a new process for generating 3D batteries was developed at the Kalsruhe Institute of Technology (KIT): patterning of thin and thick film electrodes by direct laser modification and ablation. KIT introduced a new battery design concept which was successfully assigned to the 3D-concept ("3D Battery") for achieving large areal energy capacities and power densities [8, 68-70]. This concept is not limited to micro-batteries only since it can be applied to the other technical approaches listed in [8]. That means that batteries which combine high power densities and high energy density at the same time can be realized through the application of laser annealing (LA) and laser structuring (LS) processes.

14.5.1 *LA and LS of Thin Film Electrodes*

A rather new application field for laser material processing is the development of 3D structures in lithium-ion batteries based on nano-scaled materials and thin films [71-82]. For this purpose, laser annealing and laser structuring of thin film electrodes made of $LiCoO_2$, SnO_2 and $LiMn_2O_4$ were recently investigated. Lithium cobalt oxide ($LiCoO_2$) is an appropriate model system, because it is a well stablished and still the most commonly used cathode material in lithium-ion batteries [83]. $LiMn_2O_4$ and SnO_2 were studied in detail in order to investigate chemical and mechanical degradation effects in electrode materials. Furthermore, the passivation of laser generated 3D $LiMn_2O_4$ surfaces with thin films such as indium tin oxide (film thicknesses of 10-50 nm) has also been investigated with respect to a reduction of chemical degradation during electrochemical cycling.

14.5.1.1 *Laser annealing LA*

Laser annealing (LA) was successfully applied to structured and unstructured $LiCoO_2$ and $LiMn_2O_4$ thin films [76,79] in order to adjust the crystalline phase and grain size. In case of $LiCoO_2$ it was shown that suitable annealing temperatures are in the range of T=400-700 °C. Temperatures lower or equal to 400 °C lead to an insufficient phase conversion, while temperatures equal or above 700 °C led to the formation of a contamination phase (Co_3O_4). Laser annealing processes were also developed for rf magnetron sputtered lithium manganese oxide (Li-Mn-O) thin films with the aim to form a spinel-like phase [80]. The Raman spectrum for an as-deposited Li-Mn-O thin film is depicted in Fig. 14.10(a),(ii). Applying an annealing temperature of T = 600 °C for t = 100 s on the film, significant changes within the Raman spectra could be observed (Fig. 14.10(a),(iii)). The characteristic peaks for the electrochemical inactive Li_2MnO_3 phase could be assigned [84,85]. With an increase in laser annealing temperature up to T = 680 °C and a fixed annealing time of t = 100 s (Fig. 14.10(a),(iv)), Raman spectroscopy indicates a spinel-like Li-Mn-O phase showing the typical bands which indicate stretching vibrations of manganese and oxygen compounds at 629 cm^{-1} (A_{1g} species), the shoulder around ~ 590 cm^{-1} (F_{2g}) as well as a weak band at 482 cm^{-1} (F_{2g} species) [84,86]. The intensity of the shoulder around 583 cm^{-1} can be correlated with the average oxidation state of manganese and

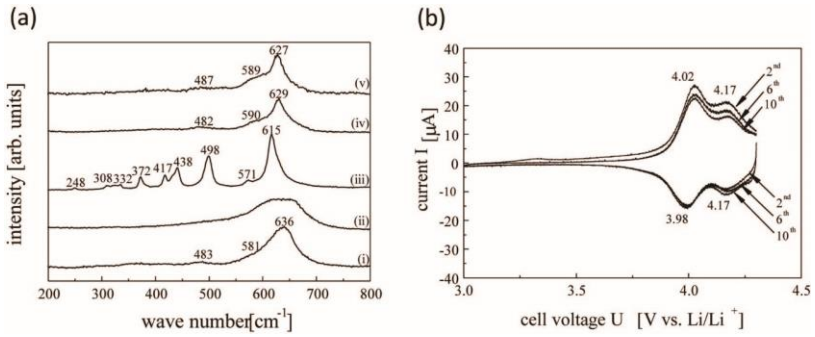

Figure 14.10. Effect of laser annealing on crystallinity and electrochemical performance; (a): Raman spectra of $Li_{0.88}Mn_{1.98}O_4$ thin films (ii-v) and $LiMn_2O_4$ reference powder (i), as-deposited film (ii), laser annealing was performed for t = 100 s at T = 600 °C (iii), for t = 100 s at T = 680 °C (iv) as well as for t = 2000 s at T = 600 °C under ambient air (v); (b): Cyclic voltammograms ($Li_{0.88}Mn_{1.98}O_4$, laser annealed for t = 2000 s at T = 600 °C). Reprinted from [80], Copyright (2012), with permission from Elsevier.

therefore increases upon de-intercalation of lithium [84]. This could be one reason for differences between the spectra for annealed films with the reference powder (Fig. 10(a)(i)) when taking into account the lithium deficiency of the sputtered thin film. Similar Raman spectra could be observed for an annealing temperature of T = 600 °C by applying an annealing time of t = 2000 s (Fig. 14.10(a),(v)). The thin films showing the spinel phase were cycled and analyzed with respect to the composition of the formed solid-electrolyte interface (SEI) layer [80]. Cyclic voltammetry or CV scans identified that film annealing at T = 600 °C for t = 2000 s leads to characteristic redox peaks for spinel thin films (Fig. 14.10(b)). SEM and XPS analysis showed that the SEI layer was formed on top of a laser annealed spinel-like cathode surface [80].

14.5.1.2 *Laser structuring (LS) of $LiCoO_2$ thin films*

LS of $LiCoO_2$ can be realized via classical laser direct ablation or via self-organized structuring (Fig. 14.11). The formation of laser-induced self-organized conical surface structures on $LiCoO_2$ thin films can be explained by selective material ablation and subsequent material re-deposition [71,76]. In recent research it was nearly possible to avoid material loss during patterning while the height of the created cones could be increased up to 8.4 µm for thin film thickness of 3 µm. Appropriate surface structures and orientations of lithium intercalation planes should increase lithium diffusion significantly [87]. The free standing microstructures (Fig. 14.11) contain little residual stress and expansion during electrochemical cycling can be easily compensated, leading to reduced crack formation and better cycling stability [88]. In [89] the transfer of that structuring

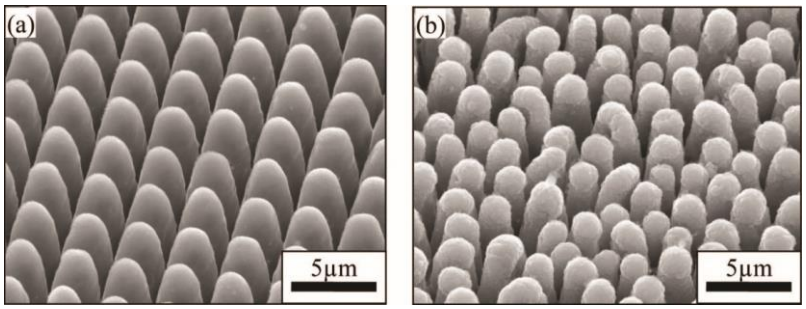

Figure 14.11. SEM images of laser structured $LiCoO_2$ thin films using mask imaging (a) with a laser fluence of 3 J/cm² and self-organized surface structures (b) with laser fluences of 0.5 J/cm² and 2 J/cm². 60 laser pulses at a repetition rate of 100 Hz were applied. Reprinted from [81], Copyright (2012), with permission from Elsevier.

technology to thick films made of $LiCoO_2$ tape cast electrodes was successfully demonstrated.

Electrochemical cycling was applied to laser structured and unstructured thin films. The theoretical capacity of 140 mAh/g was used for the calculation of the C-rate. The C-rate is a measure of the rate at which a battery is charged/ discharged relative to its maximum capacity. A "1C" rate means that the discharge current will discharge the entire battery in 1 hour. To analyze the high power capability of the samples, the charging current was increased stepwise. After eleven charge/discharge cycles at C/20 the current rate was increased to C/5 for another eleven cycles. Finally, 100 cycles at 1C were measured. The results are shown in Fig. 14.12. The unstructured films showed a higher initial discharge capacity compared to the structured and laser annealed films. After eleven cycles at the lowest charging rate the capacity dropped 27%. During the next cycles at C/5 a further decrease in capacity of 31% was measured. After a few cycles at 1C the capacity was reduced below 5 mAh/g. Although the initial capacity of the laser structured thin films was lower, the capacity increased to about 140 mAh/g during the first five cycles. This may be due to run-in effects (e.g. formation of solid

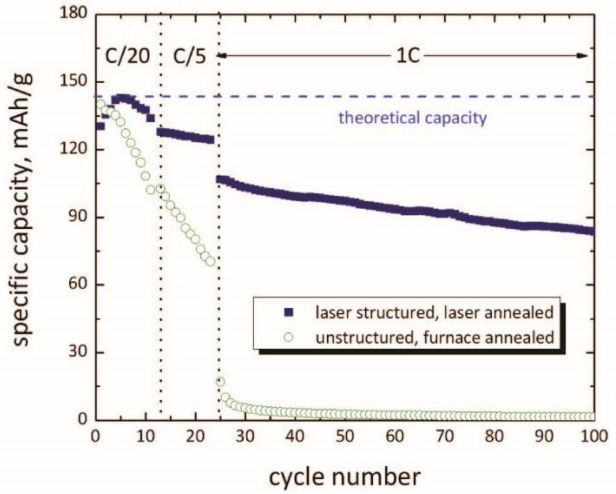

Figure 14.12. Discharge capacity as a function of the cycle number of unstructured and laser structured $LiCoO_2$ thin films after furnace annealing for 3 h or laser annealing at 600°C for 250 s, respectively. Laser structuring was performed with a wavelength λ = 248 nm in ambient air. [90] with permission of Springer.

electrolyte interphase). During the eleven cycles at the lowest current rate the capacity of the structured thin film increased about 3%. At C/5 a slight decrease in capacity of 3% could be observed. After 100 cycles at 1C the capacity reached values of 78 mAh/g. The improvement of battery performance by laser structuring can be attributed to different processes. Through the increased surface area of the structured films more lithium diffusion planes are accessible which in turns leads to a higher lithium diffusion rate at high charging rates. This leads to a maximum lithium diffusion length of 1 µm which is significantly smaller than the maximum diffusion length of 3.5 µm of the unstructured films. Concomitantly, the free standing cones contain little residual stress and expansion during electrochemical cycling can be easily compensated, leading to reduced crack formation and better cycling stability.

14.5.1.3 *Laser structuring of SnO_2 thin films*

Laser structuring was also applied for SnO_2 thin film anode (see Fig. 14.13). The periodic structures had a height of 3 µm and a pitch distance down to 4 µm. The minimum spacing between periodical arranged structures was 400 nm (Fig. 14.13,

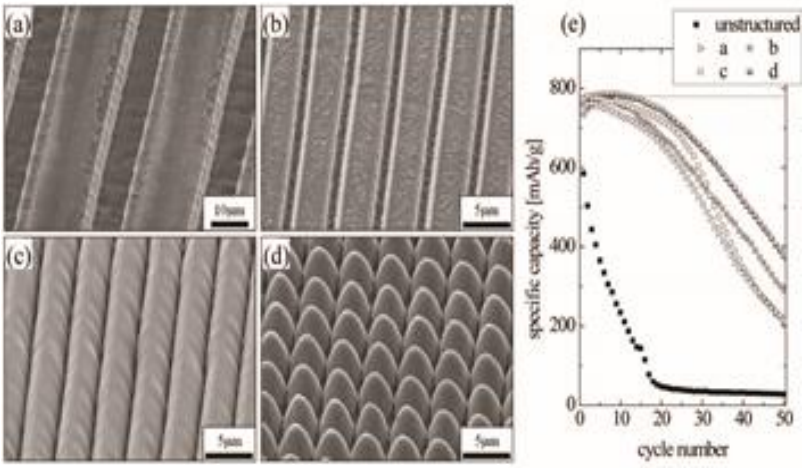

Figure 14.13. (a-d) SEM-images of laser structured SnO_2 thin films with different structure sizes. (e) Corresponding specific discharge capacity of laser structured SnO_x thin film electrodes as function of cycle number at a charge/discharge rate of C/2.

c, d). The ablated grooves (Fig.14.13, a, b) had a width of 2-10 µm and a pitch distance of 5-40 µm. The results of electrochemical cycling between 0.02 V and 1.2 V at a charge/discharge rate of C/2 are depicted in Fig. 14.13(e). The unstructured thin film shows poor cycling behaviour with the capacity of less than 50 mAh/g after 20 cycles. In comparison, the laser structured thin films exhibited significantly better performance. Capacities of > 700 mAh/g - which are in good agreement to the theoretical capacity - could be obtained for more than 20 cycles. After 50 cycles, capacities between 200 mAh/g and 400 mAh/g could be retained. It becomes clear that even for the line structures with structure sizes of 20 µm, a considerable improvement of battery performance is observed. This result suggests that significant mechanical stress is formed throughout the thin film, which can be reduced by applying free-standing structures (during cycling of SnO_2: volume changes up to 359 % are expected). A reduction of structure dimension leads to further improvement of cycling stability, while the best results were obtained for the free-standing conical structures shown in Fig. 14.13(d).

14.5.1.4 *Laser structuring (LS) of $LiMn_2O_4$ thin films*

Figure 14.14 shows the result of the laser patterning process on $LiMn_2O_4$ cathode thin films using a grating mask. Spherical surface structures were formed with smooth surfaces and without any debris. Laser ablation was performed under ambient air using a laser fluence of $\varepsilon = 1.6$ J/cm^2, N = 60 laser pulses and a repetition rate of $\nu_{rep} = 100$ Hz. Figure 14.15 shows a cross-sectional Focused Ion

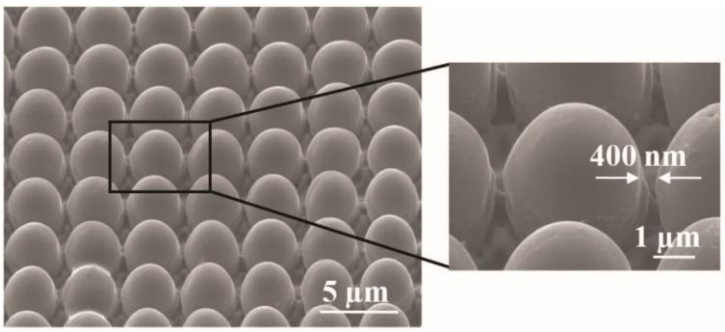

Figure 14.14. Spherical 3D surface structures formed via direct laser structuring of Li-Mn-O thin films ($\lambda = 248$ nm, energy density $\varepsilon = 1.6$ J/cm^2, pulse number N = 60, repetition rate $\nu_{rep} = 100$ Hz, ambient air). Reproduced from Ref. [91] with permission from JLMN publisher.

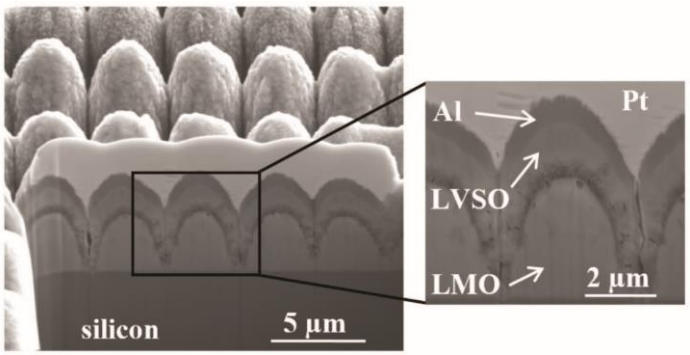

Figure 14.15. Cross-sectional FIB image showing the principle set-up of a 3-dimensional all-solid state cell grown by rf magnetron sputtering of lithium vanadium silicon oxide (LVSO) electrolyte and aluminum (Al) anode material on top of the laser generated spherical lithium manganese oxide (LMO) structures. Reproduced from Ref. [91] with permission from JLMN publisher.

Beam (FIB) image of the laser-structured all-solid state cell grown by rf sputtering. First, a 3.3 µm thick Li-Mn-O cathode (LMO) was sputter-deposited on silicon. Silicon substrate was used in order to break the sample for cross-sectional views. Within the laser patterning process 3-dimensional spherical surface structures were formed. In a third and fourth step, lithium vanadium silicon oxide (LVSO) was used as solid electrolyte as well as aluminum (Al) was deposited on top of the surface structures with a maximum LVSO layer thickness of about 1.4 µm and a maximum Al layer thickness of about 700 nm. The challenge was to reach a complete coverage of these materials to the cathode and besides sporadic cracks this could be achieved in a first experimental approach. For the FIB procedure Platinum (Pt) was deposited on top of the 3D structures. The combination of laser patterning processes and rf magnetron sputtering can be realized to achieve new 3D battery designs.

14.5.2 *LS of Thick Film Electrodes*

The electrodes, anodes and cathodes, in state-of-the-art LIBs are complex multi-material systems that are provided with defined material components, grain sizes, porosities, and pore size distributions in the micrometer and sub-micrometer ranges. Thick film electrodes are formed from slurries of active material powders, binders, solvents and additives and are fed to coating machines to be deposited on

current collector foils. Thick film electrodes reveal a high porosity in the range of 30-50 % which is necessary in order to enable suitable wetting of the active material with liquid electrolyte. The active material and other constituents are mixed by battery manufacturers according to special and generally inaccessible recipes. Currently, secondary lithium-ion cells utilize cathode materials such as layered compounds like $Li(Ni_{1/3}Mn_{1/3}Co_{1/3})O_2$ (NMC), $LiFePO_4$ (LFP) or $LiCoO_2$ (LCO). Differences can be found in the type of lithium diffusion paths: the olivine-type LFP and some silicon derivatives provide 1-dimensional paths whereas the layered compounds 2-dimensional and the spinel-type 3-dimensional path. Another distinction can be the kinetic of the diffusion. The practical capacities also differ within those materials, counting 148 mAh/g for NMC, 140 mAh/g for LCO and 130 mAh/g for LFP. As counter electrode, graphite anodes are used in state-of-the-art LIBs with a practical capacity of about 330 mAh/g.

Due to the fact that a significant amount of inactive material such as metallic current collector, separator material, binder, carbon black, liquid electrolyte and pouch material (for cells with pouch cell design) are used in a state-of-the-art lithium-ion cell, the gravimetric energy density is rather low. While on material level (NMC) a gravimetric energy density of about 650 Wh/kg can be reached, the practical energy density drops down to values in the range of 100-150 Wh/kg. For a successful and economic use of LIBs in future lightweight actuating device a significant increase of the practical energy density is required. It is assumed that only a systematic and concerted approach on material level ("material challenge") and cell architecture ("engineering challenge") can achieve such high energy

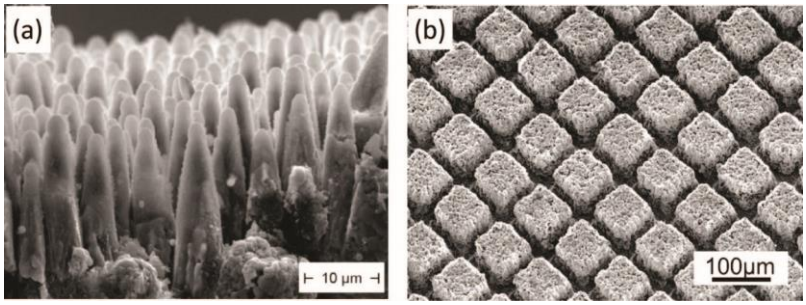

Figure 14.16. SEM of micro-structures laser-generated in composited electrode cathode materials: Self-organized microstructures by excimer laser ablation (a) and micro-pillars obtained by direct fs-laser laser structuring (b) [93].

densities in the range or above 300 Wh/kg. The development of 3D electrode architectures in thick film electrodes is a rather new approach for improving battery performance. For this purpose, we established different types of laser processing for increasing the active surface area, i.e., 'laser-assisted self-organizing structuring' and 'direct structuring' (Figure 14.16). The first step of these processes can be applied to thin films and thick-film electrodes that have small electrode footprint areas (coin cells). The second process is suitable for small and large electrode footprint areas (pouch cells). We used excimer laser ablation at a wavelength of 248nm to produce self-organized surface structures (Fig. 14.16a) on lithium cobalt oxide and NMC thick film electrodes. We also applied direct laser structuring - either with a 200 ns fiber laser or an ultrafast fiber laser (380fs) - to form 3D microstructures (Fig. 14.16b) [92].

14.5.3 *LS Turns Electrodes into Superwicking*

A main issue in cell production is the electrolyte wetting of LIBs which is realized by time and cost consuming vacuum and storage processes at elevated temperatures [94]. The liquid electrolyte has to be forced into micro- and nano-sized pores of the composite electrode material (Fig. 14.17). In fact, the use of current electrolyte filling processes result in insufficient wetting of the electrode surfaces, which is one drawback leading to certain rate of production failure, lowered cell capacity or reduced battery life-time. At KIT, a cost efficient laser-based technology for the realization of micro capillary structures in separators [95] and thick-film tape-cast electrodes was developed to achieve a tremendous acceleration of the wetting process and to shorten the time-span for cell manufacturing. For thick film composite electrodes an appropriate structure design delivers the most efficient capillary transport [96]. Electrochemical analysis showed that a steep rise of capacity retention at high charging and discharging currents and an improved cell life-time can be obtained in comparison to standard cells with unstructured battery materials. This significant increase in battery lifetime is caused by efficient and instantaneous liquid electrolyte transport that is enabled by the laser-generated micro-capillary structures. The laser-generated capillary structures in electrode materials increase cell reliability and shorten battery production times. Improved cycle lifetimes and increased capacity retention also mean that high-power batteries for second-life applications become a possibility.

Electrodes with laser structured 3D architectures can provide a homogeneous and fast wetting behavior (Fig. 14.17b) and finally lead to an improved

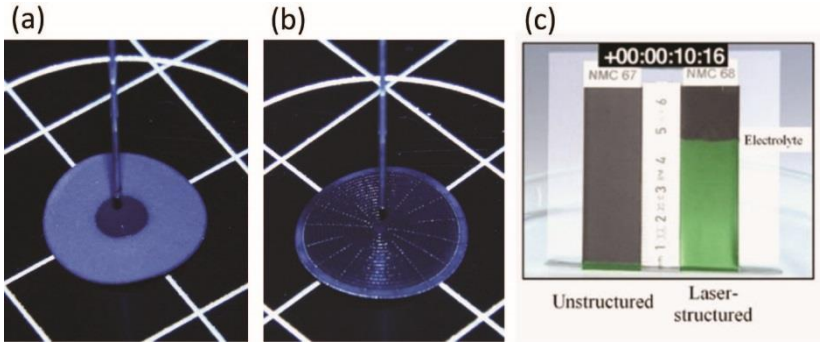

Figure 14.17. Liquid electrolyte wettability of NMC thick film electrodes: Single-drop-electrolyte (3 µl) wetting behavior on unstructured (a) and laser structured (b) thick film electrodes. Snap-shot (c) of video imaging the capillary rise in dependence of wetting time (~ 10 s).

electrochemical performance. The capillary rise of liquid electrolyte in thick film electrodes (Fig. 14.17c) can be very well described by the classical Washburn equation, which is described elsewhere [96]. For the formation of capillary structures, ns-laser ablation as well as ultrafast laser processing were investigated. For ns-laser radiation (λ=1064 nm, pulse length 200 ns) the laser beam energy is absorbed at the material surface and due to heat conduction the temperature of the surrounding composite material increases. The binder material used for tape cast electrodes (~5 wt%) is Polyvinylidenfluoride (PVDF), which has a low decomposition temperature in the range of 250 – 350 °C [97]. Therefore, the PVDF binder matrix spontaneously evaporates and active particles are removed from the laser beam interaction zone. A similar ablation process for metal/polymer composite materials has already been described by Slocombe *et al*. [98]. Nanosecond laser ablation is not appropriate for each type of electrode material. For example, ns-laser structuring of LFP electrodes leads to melt formation and therefore to an undesired modification of the active material. Therefore, the use of ultrafast laser materials processing is necessary for this type of material. Furthermore, the ablation efficiency of LFP increases by a factor of 3 by using femto- or picosecond laser ablation in comparison to ns-laser ablation [99]. For battery production costs it is important to reduce the amount of ablated material which in turn means that small capillary widths and high aspect ratios are

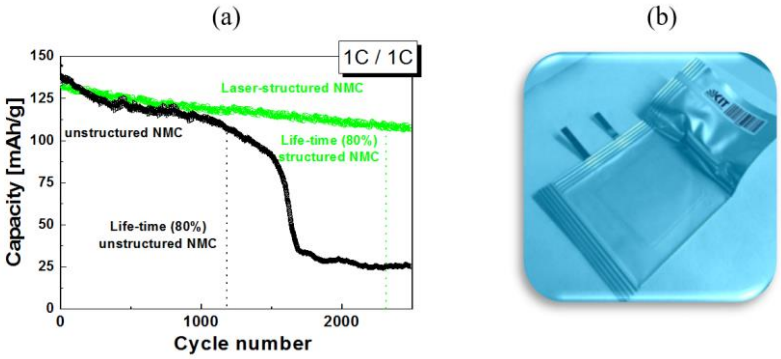

Figure 14.18. Specific discharge capacities (a) of NMC pouch cells (b) with laser structured and unstructured electrodes as function of cycle number (1 C charge/1 C discharge) Reproduced from Ref. [96] with permission from The Royal Society of Chemistry.

preferred. By using ultrafast laser ablation, it is shown that the aspect ratio can be significantly increased and that the loss of active material can be reduced from 20 % down to values below 5 % [100]. At KIT, this structuring process was conducted under ambient air conditions, and the ablated material was removed through an exhaust.

Capacity retention and cell life-time can be illustrated by plotting the discharge capacity as a function of cycle numbers for lithium-ion cells with both the laser-structured and unstructured NMC electrodes (Fig. 14.18). The discharge capacity of the laser-structured NMC cell drops to 80 % of the initial capacity after 2290 cycles (Fig. 14.18) while for the lithium-ion cell with unstructured electrodes the cell life-time (80% of its initial capacity) is reached after only 1140 cycles. Furthermore, the discharge capacity of the cell with the laser-structured NMC electrode reaches a value of 108 mAh/g after 2290 cycles, indicating that efficient liquid electrolyte transport improves the electrochemical performance for these cells. These benefits are achieved without cost- and time-consuming storage steps thanks to the micro capillary structures produced by laser structuring of the electrodes.

14.6 CHALLENGES AND FUTURE DIRECTIONS

Although laser-based processing techniques have been successfully employed for the fabrication of energy storage systems, these techniques present certain challenging issues. Three of the most relevant challenges are presented in the following paragraphs.

First of all, the thickness of the PLD grown electrodes is limited to less than a few microns due to the increased internal cell resistance characteristic of vapor deposited electrode films. Thus, the capacity of the thin film microbatteries are not sufficient to operate many microelectronic devices. One possible way to increase the electrode thickness with relatively low internal resistance loss might be through co-deposition of conductive carbon with the cathode and anode materials by alternatively ablating carbon and electrode targets during PLD. This carbon containing electrodes would enhance the conductivity of the electrodes, reducing the internal cell resistance loss, and allowing improved capacity.

Another challenging issue in designing micro scale batteries is to develop appropriate packaging processes that can achieve a reliable seal to protect the electrode materials with minimum weight and volume. Typical commercial coin cell batteries may not be used as micropower sources in many microelectronic devices due to their larger volume. In this matter, microbatteries can be designed to be embedded within the laser machined pockets on a chip. LIFT processes are practical and easily customizable, since they can print battery materials directly on top of devices and they can also fabricate pockets for embedded microbatteries. Thus, the LIFT techniques will play an important role in the development of next generation of microelectronic devices.

Finally, integration of the microbatteries into other microelectronic devices on a chip must be achieved for the development of advanced microelectronic devices. One of main challenge to achieve this goal is to develop leak-free electrolytes, such as solid-state composite polymer electrolytes. Although PLD and LIFT techniques were successfully utilized to produce solid-state electrolytes, the ionic conductivity of these solid-state electrolytes is lower than that of liquid electrolytes, which may lower the energy density of the resulting microbatteries. Thus, considerable research on developing solid-state electrolytes with improved properties will be required to produce the micropower sources used for the next generation of microelectronic devices.

14.7 SUMMARY

We have reviewed three laser-based processing techniques for the fabrication of energy storage and power generation devices. Firstly, the use of PLD technique

was described to deposit numerous types of cathodes, anodes and solid-state electrolytes for thin-film microbatteries. By applying sequential PLD processes, all-solid state thin-film microbatteries were successfully fabricated. Secondly, the use of LIFT techniques was demonstrated to print active electrochemical materials for the fabrication of various micropower systems, including ruthenia-based planar ultracapacitors, rechargeable thick-film Li-ion microbatteries and solid-state electrolyte membranes. The LIFT process was also utilized to print sequential layers of cathode, solid-state electrolyte, and anode layers inside laser-micro-machined pockets to build embedded all-solid-state Li-ion microbatteries. Thirdly, the laser structuring and laser annealing processes were applied to build 3D architectures into thin-film and thick film electrodes for Li-ion microbatteries, which improved their electrochemical performance including cycling and high current discharge rate by increasing their overall active surface area.

As described in the Introduction, laser-based processes have been realized as practical techniques to integrate energy storage and micro power sources with microdevices. In principle, these laser-based processes can be used at the beginning, during or after the fabrication of a device. For example, with PLD the growth of thin films would most likely take place at the beginning of the device fabrication steps, since the films will have to be patterned after deposition and other steps will be required before a device can be produced. On the other hand, the LIFT process can be applied at any stage of the fabrication sequence, even after the device has been completed, since the LIFT is additive and non-lithographic in nature. Thus, laser printing of a microbattery for a particular device could take place after the device is already manufactured, allowing the embedding of micropower sources into existing devices. Finally, laser surface modification, such as LS and LA, can be applied at any stage of the fabrication process and can be applied to only a specific region of a structure or device, which opens a wide range of possibilities. Such flexibility and adaptability make the use of laser-based processing techniques for energy storage applications highly applicable for solving the challenge of developing fully integrated autonomous microelectronics.

Acknowledgments

This work was supported by the Office of Naval Research (ONR) through the Naval Research Laboratory Basic Research Program. Special thanks to Dr. Mike Ollinger and Dr. Tom Sutto for their help in the fabrication of embedded microbatteries and solid-state electrolytes, Ray Auyeung for his help with LIFT

process, and Dr. Johannes Proell for his great contributions in developing the laser structuring and laser annealing processes of battery materials. This work has been financially supported by "FabSurfWar - Design and Fabrication of Functional Surfaces with Controllable Wettability, Adhesion and Reflectivity" (Funded under: H2020-EU.1.3.3, project reference: 644971) from the European Commission under Horizon 2020 Programme (H2020). Finally, the support for laser processing by the Karlsruhe Nano Micro Facility (KNMF, http://www.knmf.kit.edu/) a Helmholtz research infrastructure at the Karlsruhe Institute of Technology (KIT) is gratefully acknowledged.

References

1. Mazor, H., Golodnitsky, D., Bustein, L., Gladkich, A., and Peled, E. (2012). Electrophoretic deposition of lithium iron phosphate cathode for thin-film 3D-microbatteries, *J. Power Sources* **198**, pp.264-272.
2. Wang, C., Zheng, W., Yue, Z., Too, C. O., and Wallace, G. G. (2011). Buckled, stretchable polypyrrole electrodes for battery applications, *Adv. Mat.* **23**, pp.3580-3584.
3. Sun, K., Wei, T.-S., Ahn, B. Y., Seo, J. Y., Dillon, S. J., Lewis, J. A. (2013). 3D printing of interdigitated Li-ion microbattery architectures, *Adv. Mat.* **25**, pp.4539-4543.
4. Bates, J., Dudney, N. J., Neudecker, B., Ueda, A., and Evans, C. D. (2000). Preferred orientation of polycrystalline $LiCoO_2$ films, *J. Electrochem. Soc.***147**, pp.59-70.
5. Wang, Z. L. (2010). Toward self-powered sensor networks, *Nano Today* **5**, pp.512-514.
6. Beidaghi, M. and Gogotsi, Y. (2014). Capacitive energy storage in micro-scale devise: recent advances in design and fabrication of micro-supercapacitors, *Energy Environ. Sci.* **7**, pp.867-884.
7. Koeneman, P. B., Busch-Vishniac, I. J., and Wood, K. L. (1997). Feasibility of micro power supplies for MEMS, *J. Microelectromech. Sys*. **6**, pp. 355–362.
8. Ferrari, S., Loveridge, M. Beatti, S. D. Jahn, M., Dashwood, R. J. Bhagat, R. (2015). Latest advances in the manufacturing of 3D rechargeable lithium microbatteries, *J. Power Sources* **286**, pp. 25-46.
9. Oudenhoven, J. F. M., Baggetto, L., and Notten, P. H. L. (2011). All-Solid-State Lithium-Ion Microbatteries: A Review of Various Three-Dimensional Concepts, *Adv. Energy Mater.* **1**, pp.10-33.
10. Jeyaseelan, A. V. and Rohan, J. F. (2009). Fabrication of three-dimensional substrates for Li microbatteries on Si, *Appl. Surf. Sci.* **256**, pp. S61-S64.

11. Sutto, T. E., Ollinger, M., Kim, H., Arnold, C. B., and Piqué, A. (2006). Laser transferable polymer-ionic liquid separator/electrolytes for solid-state rechargeable lithium-ion microbatteries, *Electrochem. Solid-State Lett.* **9**, pp. A69-A71.
12. Simon, P. and Gogotsi, Y. (2008). Materials for electrochemical capacitors, Nat. *Mater.* **7**, pp. 845-854.
13. Nitta, N., Wu, F., Lee, J. T. and Yushin, G. (2015). Li-ion battery materials: present and future, *Materials Today* **18**, pp.252-264.
14. Goriparti, S., Miele, E., De Angelis, F., Fabrizio, E. D., Zaccaria, R. P., and Capiglia, C. (2014). Review on recent progress of nanostructured anode materials for Li-ion batteries, *J. Power Sources* **257**, pp. 421-443.
15. Eason, R. (2006) *Pulsed Laser Deposition of Thin Films*, (Wiley, New York).
16. Chrisey, D. B. and Hubler, G. K. (1994) *Pulsed Laser Deposition of Thin Films*, (Wiley, New York).
17. Phipps, C. R. (2006) *Laser Ablation and its Applications*, (Springer, New York).
18. Julien, C., Haro-Poniatowski, E., Camacho-Lopez, M.A., Escobar-Alarcon, L., and Jimenez-Jarquin, J. (2000). Growth of LiMn2O4 thin films by pulsed laser deposition and their electrochemical properties in lithium microbatteries, *Mat. Sci. Eng. B* **72**, pp. 36-46.
19. Iriyama, Y., Inaba, M. Abe, T., and Ogumi, Z. (2001) Preparation of c-axis oriented thin films of LiCoO2 by pulsed laser deposition and their electrochemical properties, *J. Power Sources* **94**, pp. 175-182.
20. Xia, H., Lu, L., and Ceder, G. (2006). Substrate effect on the microstructure and electrochemical properties of LiCoO2 thin films grown by PLD, *J. Alloys and Compounds* B pp. 304-310.
21. Kim, W. S. (2004). Characteristics of LiCoO2 thin film cathodes according to the annealing ambient for the post-annealing process, *J. Power Sources* **134**, pp.103-109.
22. Kuwata, N., Kumar, R., Toribami, K. Suzuki, T., Hattori, T. and Kawamura, J. (2006). Thin film lithium ion batteries prepared only by pulsed laser deposition, *Solid State Ionics* **177**, pp.2827-2832.
23. Xia, H. and Lu, L. (2007). Texture effect on the electrochemical properties of LiCoO2 thin films prepared by PLD, *Electrochim. Acta* **52**, pp. 7014-7021.
24. Xia, H., Lu, L., and Meng, Y. S. (2008). Growth of layered $LiNi_{0.5}Mn_{0.5}O_2$ thin films by pulsed laser deposition for application in microbatteries, *Appl. Phys. Lett.* **92**, pp. 011912.
25. Simmen, F., Lippert, T., Novák, P., Neuenschwander, B., Döbeli, M., Mallepell, M., Wokaun, A. (2008). The influence of lithium excess in the target on the properties and compositions of Li1+xMn2O4-δ, *Appl. Phys. A.* **93**, pp.711-716.
26. Perkins, J. D., Bahn, C. S., Parilla, P. A., McGraw, J. M., Fu, M. L., Duncan, M., Yu, H., and Ginley, D. S. (1999). $LiCoO_2$ and LiCo1-xAlxO2 thin film cathodes grown by pulsed laser ablation, *J. Power Sources* **81-82**, pp.675-679.

27. Wang, G. X., Lindsay, M. J., Ionescu, M., Bradhust, D. H., Dou, S. X., and Liu, H. K. (2001). Physical and electrochemical characterization of $LiNi_{0.8}Co_{0.2}O_2$ thin-film electrodes deposited by laser ablation, *J. Power Sources* **97-98**, pp. 298-302.
28. Ramana, C. V., Zaghib, K., and Julien, C. M. (2007). Pulsed-laser deposited $LiNi_{0.8}Co_{0.15}Al_{0.05}O_2$ thin films for application in microbatteries, *Appl. Phys. Lett.* **90**, pp. 021916.
29. Lu, Z. G., Lo, M. F., and Chung, C. Y. (2008). Pulsed laser deposition and electrochemical characterization of $LiFePO_4$-C composite thin films, *J. Phys. Chem.* **112**, pp. 7069-7078.
30. Yan, B., Liu, J., Song, B., Xiao, P., and Lu, L. (2013). Li-rich thin film cathode prepared by pulsed laser deposition," *Scientific Reports* **3**, pp.3332:1-5.
31. Biserni, E., Xie, M., Brescia, R., Scarpellini, A., Hashempour, M., Movahed, P., George, S.M., Bestetti, M., Li Bassi, A., Bruno, P. (2015). Silicon algae with carbon topping as thin-film anodes for lithium-ion microbatteries by two-step facile method, J. Power Sources 274, pp-252-259.
32. Radhakrishnan, G., Adams, P. M., Foran, B., Quinzio, M. V., and Brodie, M. J. (2013). Pulsed laser deposited Si on multilayer graphene as anode material for lithium ion batteries, *APL Materials* **1**, pp. 062103:1-6.
33. Kuwata, N., Kawamura, J., K. Toribami, K., T. Hattori, T., and Sata, N. (2004). Thin-film lithium-ion battery with amorphous solid electrolyte fabricated by pulsed laser deposition, *Electrochem. Commum.* **6**, pp. 417-421.
34. Goriparti, S., Miele, E., De Angelis, F., Di Fabrizio, E., Zaccaria, R. P., and Capiglia, C. (2014). Review on recent progress of nanostructured anode materials for Li-ion batteries, *J. Power Sources* **257**, pp. 421-443.
35. Ryu, J. H., Kim, J. W., Sung, Y. E., and Oh, S. M. (2004). Failure modes of silicon powder negative electrode in lithium secondary batteries, *Electrochemical and Solid-State Letters* **7**, pp.A306-A309.
36. Zhao, S., Fu, Z., and Qin, Q. (2002). A solid-state electrolyte lithium phosphorus oxynitride film prepared by pulsed laser deposition, *Thin Solid Films* **415**, pp. 108-113.
37. Zhao, S. and Qin, Q. (2003). Li-V-Si-O thin film electrolyte for all-solid-state Li-ion battery, *J. Power Sources* **122**, pp.174-180.
38. Kawamura, J., Kuwata, N., Toribami, K., Sata, N., Kamishma, O., and Hattori, T. Preparation of amorphous lithium ion conductor thin films by pulsed laser deposition, *Solid State Ionics* **175**, pp.273-276.
39. Ohta, N., Takada, K., Osada, M., Zhang, L., Sasaki, T., and Watanabe, M. (2005). Solid electrolyte, thio-LISICON thin film prepared by pulsed laser deposition, *J. Power Sources* **146**, pp.707-710.
40. Sakurai, Y., Sakuda, A., Hayashi, A., and Tatsumisago, M. (2011). Preparation of amorphous Li_4SO_4-Li_3PO_4 thin films by pulsed laser deposition for all-solid-state lithium secondary batteries, *Solid State Ionics* **182**, pp.59-63.

41. Sakuda, A., Hayashi, A., Hama, S., and Tatsumisago, M. (2010). Preparation of highly lithium-ion conductive $80Li_2S$-$20P_2O_5$ thin-film electrolytes using pulsed laser deposition, *J. Am. Ceram. Soc.* **93**, pp. 765-768.
42. Kim, H., Auyeung, R. C. Y., and Piqué, A. (2007). Laser-printed thick-film electrodes for solid-state rechargeable Li-ion microbatteries, *J. Power Sources* **165**, pp. 413-419.
43. Ollinger, M., Kim, H., Sutto, T. E., and Piqué, A. (2006). Laser Direct-Write of Polymer Nanocomposite, *Appl. Sur. Sci.* **252**, pp. 8212-8216.
44. Ollinger, M., Kim, H., Sutto, T. E., Martin, F., and Piqué, A. (2006) Laser printing of nanocomposite solid-state electrolyte membranes for Li micro-batteries, *JLMN-Journal of Miro/Nanoenineering* 1, pp. 102-105.
45. Kim, H., Proell, J., Kohler, R., Pfleging, W., and Piqué, A. (2012). Laser-printed and processed $LiCoO_2$ cathode thick films for Li-ion microbatteries, *JLMN-Journal of Miro/Nanoenineering* **7**, pp. 320-325.
46. Arnold, C. B., Wartena, R.C., Pratap, B., Swider-Lyons, K. E., and Piqué, A. (2002). Direct writing of planar ultracapacitor by laser forward transfer processing, *Proc. SPIE* **4637**, pp. 353-60.
47. Wartena, R.C., Curtright, A. E., Arnold, C. B., Piqué, A., and Swider-Lyons, K. E. (2004). Li-ion microbatteries generated by a laser direct-write method, *J. Power Sources* **126**, pp. 193-202.
48. Kim, H., Kushto, G. P., Arnold, C. B., Kafafi, Z. H., and Piqué, A. (2004). Laser processing of nanocrystalline TiO_2 for dye-sensitized solar cells, *Appl. Phys. Lett.* **85**, pp. 464-466.
49. Kim, H., Auyeung, R.C.Y., Ollinger, M., Kushto, G. P., Arnold, C. B., Kafafi, Z. H., and Piqué, A. (2006). Laser-sintered mesoporous TiO2 electrodes for dye-sensitized solar cells, Appl. Phys. A. **83**, pp. 73-76.
50. Piqué, A., Auyeung, R. C. Y., Kim, H., Metkus, K. M., and Mathews, S. A. (2008). Digital Microfabrication by Laser Decal Transfer, *J. Laser Micro/Nanoeng* **3**, pp.163-169.
51. Duocastella, M., H. Kim, H., Serra, P., and Piqué, A. (2012). Optimization of laser printing of nanoparticles suspensions for microelectronic applications, *Appl. Phys. A-Mater.* **106**, pp. 471-478.
52. Arnold, C. B., Serra, P., and Piqué, A. (2007). Laser direct-write techniques for printing of complex materials, *MRS Bulletin* **32**, pp. 23-31.
53. Calvert, P. (2001). Inkjet printing for materials and devices, *Chem. Mater.* **13**, pp. 3299-3305.
54. Kang, H., Soltman, D., and Subramanian, V. (2010). Hydrostatic Optimization of Inkjet-Printed Films, *Langmuir* **26**, pp. 11568-11573.
55. Soltman, D., Smith, B., Kang, H., Morris, S. J. S., and Subramanian, V. (2010). Methodology for inkjet printing of partially wetting films, *Langmuir* **26**, pp. 15686-15693.

56. Piqué, A., Auyeung, R.C.Y., Smith, A.T., Kim, H., Mathews, S.A., Charipar, N.A., and Kirleis, M.A. (2013). Laser transfer of reconfigurable patterns with a spatial light modulator, *Proc. SPIE* **8608**, 86080K.
57. Piqué, A., Kim, H., Auyeung, R. C. Y., and Smith, A. (2013). Laser forward transfer of functional materials for digital fabrication of microelectronics, *J. Imaging Sci. Techno.* **57,** pp. 040101.
58. Wang, J., Auyeung, R. C. Y., Kim, H., Charipar, N. A., and Piqué, A. (2010). Three-dimensional printing of interconnects by laser direct-write of silver nanopastes, *Adv. Mater.* **22**, pp. 4462-4466.
59. Kim, H., Piqué, A., Charipar, K. M., Auyeung, R. C. Y., and Duocastella, M. (2013). Laser printing of conformal and multi-level 3D interconnects, *Appl. Phys. A-Mater.* **113**, pp. 5-8.
60. Kim, H., Melinger, J. S., Khachatrian, A., Charipar, N. A., Auyeung, R. C. Y., and Piqué, A. (2010). Fabrication of terahertz metamaterials by laser printing, *Opt. Lett.* **35**, pp. 4039-4041.
61. Auyeung, R. C. Y., Kim, H., Birnbaum, A. J., Zalaludinov, M., Mathews, S. A., and Piqué, A. (2009). Laser decal transfer of freestanding microcantilevers and microbridges, *Appl. Phys. A-Mater.* **97**, pp. 513-519.
62. Auyeung, R.C.Y., Kim, H., Charipar, N., Birnbaum, A., Mathews, S., and Piqué, A. (2011). Laser forward transfer based on a spatial light modulator, *Appl. Phys. A-Mater.* **102**, pp. 21-26.
63. Mathews, S.A., Auyeung, R.C.Y., Kim, H., Charipar, N.A., and Piqué, A. (2013). High-speed video study of laser-induced forward transfer of silver nano-suspensions, *J. Appl. Phys.* **114**, pp. 064910: 1-9.
64. Arnold, C. B., Wartena, R. C., Swider-Lyons, K. E., and Piqué, A. (2003). Direct-write planar microultracapacitors by laser engineering, *J. Electrochem. Soc.* **150**, pp. A571-A575.
65. Sarangapani, S., Tilak, B., and Chen, C. (1996). Materials for electrochemical capacitors, *J. of Electrochemical Society*, **143**, pp. 3791-3799.
66. Dmowski, W., Egami, T., Swider-Lyons, K.E., Love, C.T., and Rolison, D. R. (2002). Local atomic structure and conduction mechanism of nanocrystalline hydrous RuO_2 from x-ray scattering, *J. Phys. Chem. B.* **106**, pp. 12677-12683.
67. McKeown, D. A., Hagans, P. L., Carette, L. P. L., Russell, A. E., Swider, K. E., and Rolison, D. R. (1999). Structure of hydrous ruthenium oxides: Implications for charge storage, *J. Phys. Chem. B* **103**, pp. 4825-4832.
68. Long, J. W., Dunn, B., Rolison, D. R., and White, H. S. (2004). Three-dimensional battery architectures, *Chemical Reviews*, **104**(10), pp. 4463-4492.
69. Notten, P. H. L., Roozeboom, F., Niessen, R. A. H., and Baggetto, L. (2007). 3-D integrated all-solid-state rechargeable batteries, *Adv. Mater.* **19**(24), pp. 4564-4567.

70. Oudenhoven, J. F. M., Baggetto, L., and Notten, P. H. L. (2011). All-Solid-State Lithium-Ion Microbatteries: A Review of Various Three-Dimensional Concepts, *Advanced Energy Materials* **1**(1), pp. 10-33.
71. Ketterer, B., Vasilchina, H., Seemann, K., Ulrich, S., Besser, H., Pfleging, W., Kaiser, T. (2008). Development of high power density cathode materials for Li-ion batteries, *International Journal of Materials Research*, **99**(10), pp. 1171-1176.
72. Kohler, R., Besser, H., Hagen, M., Ye, J., Ziebert, C., Ulrich, S., Proell, J.(2011). Laser micro-structuring of magnetron-sputtered SnO(x) thin films as anode material for lithium ion batteries, *Microsystem Technologies-Micro-and Nanosystems-Information Storage and Processing Systems*, **17**(2), pp. 225-232.
73. Kohler, R., Bruns, M., Smyrek, P., Ulrich, S., Przybylski, M., and Pfleging, W. (2010). Laser annealing of textured thin film cathode material for lithium ion batteries, *Proc. SPIE* **7585**, pp. 75850O 1-11.
74. Kohler, R., Proell, J., Ulrich, S., Przybylski, M., and Pfleging, W. (2011). Laser processing of SnO_2 electrode materials for manufacturing of 3D micro-batteries, *Proc. SPIE* **7921**, pp. 79210P: 1-11.
75. Kohler, R., Proell, J., Ulrich, S., Trouillet, V., Indris, S., Przybylski, M., and Pfleging, W. (2009). Laser-assisted structuring and modification of $LiCoO_2$ thin films, *Proc. SPIE* **7202**, pp 720207: 1-11.
76. Kohler, R., Smyrek, P., Ulrich, S., Bruns, M., Trouillet, V., and Pfleging, W. (2010). Patterning and annealing of nanocrystalline $LiCoO_2$ thin films, *Journal of Optoelectronics and Advanced Materials*, **12**(3), pp. 547-552.
77. Proell, J., Kohler, R., Adelhelm, C., Bruns, M., Torge, M., Heißler, S., Przybylski, M., Ziebert, C, and Pfleging, W. (2011). Laser modification and characterization of Li-Mn-O thin film cathodes for lithium-ion batteries, *Proc. SPIE* **7921**, pp. 79210Q 1-14.
78. Proell, J., Kohler, R., Mangang, A., Ulrich, S., Ziebert, C., and Pfleging, W., "3D Structures in Battery Materials," JLMN-Journal of Laser Micro/Nanoengineering, 7(1), 97-104 (2012).
79. Proell, J., Kohler, R., Torge, M., Ulrich, S., Ziebert, C., Bruns, M., Seifert, H. J., and Pfleging, W. (2011). Laser microstructuring and annealing processes for lithium manganese oxide cathodes, *Applied Surface Science* **257**, pp. 9968-9976.
80. Proll, J., Kohler, R., Mangang, A., Ulrich, S., Bruns, M., Seifert, H. J., and Pfleging, W. (2012). Diode laser heat treatment of lithium manganese oxide films, *Applied Surface Science* **258**(12), pp. 5146-5152.
81. Kohler, R., Proell, J., Bruns, M., Ulrich, S., Seifert, H. J., and Pfleging, W. (2013). Conical surface structures on model thin-film electrodes and tape-cast electrode materials for lithium-ion batteries, *Applied Physics A-Materials Science & Processing*, **112**(1), pp. 77-85.
82. Proll, J., Weidler, P. G., Kohler, R., Mangang, A., Heissler, S., Seifert, H. J., and Pfleging, W. (2013). Comparative studies of laser annealing technique and furnace

annealing by X-ray diffraction and Raman analysis of lithium manganese oxide thin films for lithium-ion batteries, *Thin Solid Films* **531**, pp. 160-171.

83. Zhang, Y., Chung, C. Y., and Min, Z. (2008). Growth of HT-$LiCoO_2$ thin films on Pt-metatized silicon substrates, *Rare Metals* **27**(3), pp. 266-272.
84. Julien, C. M., and Massot, M. (2003). Lattice vibrations of materials for lithium rechargeable batteries III. Lithium manganese oxides, *Materials Science and Engineering* **100**, pp. 69-78.
85. Park, S. H., Sato, Y., Kim, J.-K., and Lee, Y.-S. (2007). Powder property and electrochemical characterization of Li_2MnO_3 material, *Materials Chemistry and Physics* **102**(2-3), pp. 225-230.
86. Julien, C. M., and Massot, M. (2003). Lattice vibrations of materials for lithium rechargeable batteries I. Lithium manganese oxide spinel, *Materials Science and Engineering* **97**, pp. 217-230.
87. Winter, R., and Heitjans, P. (2001). Li+ diffusion and its structural basis in the nanocrystalline and amorphous forms of two-dimensionally ion-conducting LixTiS2, *Journal of Physical Chemistry B* **105**(26), pp. 6108-6115.
88. Hudaya, C., Halim, M., Proll, J., Besser, H., Choi, W., Pfleging, W., Seifert, H. J., and Lee, J. K. (2015). A polymerized C-60 coating enhancing interfacial stability at three-dimensional $LiCoO_2$ in high-potential regime, *J. Power Sources* **298**, pp. 1-7.
89. Kohler, R., Proell, J., Bruns, M., Ulrich, S., Seifert, H. J., and Pfleging, W., "Conical surface structures on model thin film electrodes and tape cast electrode materials for lithium ion batteries," Applied Physics a-Materials Science & Processing, (submitted).
90. Pfleging, W., Kohler, R., Südmeyer, I., and Rohde, M. (2013). *Laser Micro and Nano Processing of Metals, Ceramics, and Polymers*, (Springer, Berlin Heidelberg).
91. Proell, J., Kohler, R., Mangang, A., Ulrich, S., Ziebert, C., and Pfleging, W. (2012). 3D Structures in Battery Materials, *Journal of Laser Micro Nanoengineering* **7**(1), pp. 97-104.
92. Kim, J. S., Pfleging, W., Kohler, R., Seifert, H. J., Kim, T. Y., Byun, D., Jung, H. G. *et al.* (2015). Three-dimensional silicon/carbon core-shell electrode as an anode material for lithium-ion batteries, *J. Power Sources* **279**, pp. 13-20.
93. Pfleging, W., Mangang, M., Zheng, Y., and Smyrek, P. (2013). Laser structuring for improved battery performance, *SPIE Newsroom*, pp. 1-3. Copyright 2013 Society of Photo Optical Instrumentation Engineers. One print or electronic copy may be made for personal use only. Systematic electronic or print reproduction and distribution, duplication of any material in this paper for a fee or for commercial purposes, or modification of the content of the paper are prohibited. http://dx.doi.org/10.1117/12.807505
94. Wood, D. L., Li, J. L., and Daniel, C. (2015). Prospects for reducing the processing cost of lithium ion batteries, *J. Power Sources* **275**, pp. 234-242.

95. Pröll, J., Schmitz, B., Niemöeller, A., Robertz, B., Schäfer, M., Torge, M., Smyrek, P. *et al.*, "Femtosecond laser patterning of lithium-ion battery separator materials: impact on liquid electrolyte wetting and cell performance," *Proc. SPIE* **9351**, 93511F-7.
96. Pfleging, W., and Proell, J. (2014). A new approach for rapid electrolyte wetting in tape cast electrodes for lithium-ion batteries, *Journal of Materials Chemistry A* **2**(36), pp. 14918-14926.
97. Choi, J., Morikawa, E., Ducharme, S., and Dowben, P. A. (2005). Comparison of crystalline thin poly(vinylidene (70%)-trifluoroethylene (30%)) copolymer films with short chain poly(vinylidene fluoride) films, *Materials Letters* **59**(28), pp. 3599-3603.
98. Slocombe, A., and Li, L. (2000). Laser ablation machining of metal/polymer composite materials, *Applied Surface Science* **154**, pp. 617-621.
99. Mangang, M., Pröll, J., Tarde, C., Seifert, H. J., and Pfleging, W. (2014). Ultrafast laser microstructuring of LiFePO4 cathode material, *Proc. SPIE* **8968**, 89680M:1-9.
100. Smyrek, P., Proll, J., Seifert, H. J., and Pfleging, W. (2016). Laser-Induced Breakdown Spectroscopy of Laser-Structured Li(NiMnCo)O_2 Electrodes for Lithium-Ion Batteries, *Journal of the Electrochemical Society* **163**(2), pp. A19-A26.